Integrated photosynthesis during fluctuating irradiance is correlated with steady-state photosynthesis for rice grown in field environments with elevated CO2 and temperature

Journal of Experimental Botany

Cai, Chuang; Yin, Xinyou; Song, Lian; Zhou, Wei; Gu, Xinyue et al

https://doi.org/10.1093/jxb/eraf179

Journal of Experimental Botany
https://doi.org/10.1093/jxb/eraf179 Advance Access Publication 4 May 2025

RESEARCH PAPER

Integrated photosynthesis during fluctuating irradiance is correlated with steady-state photosynthesis for rice grown in field environments with elevated CO_2 and temperature

Chuang Cai[1,2], Xinyou Yin[3,*], Lian Song[1,2], Wei Zhou[1,2], Xinyue Gu[1,2,4], Xiong Yang[1,2,4], Xin-Guang Zhu[5], and Chunwu Zhu[1,2,4,*]

[1] State Key Laboratory of Soil and Sustainable Agriculture, Institute of Soil Science, Chinese Academy of Sciences, Nanjing 211135, PR China
[2] University of Chinese Academy of Sciences, Nanjing 211135, PR China
[3] Centre for Crop Systems Analysis, Department of Plant Sciences, Wageningen University & Research, PO Box 430, 6700 AK Wageningen, The Netherlands
[4] University of Chinese Academy of Sciences, Yuquan Road NO. 19A, Beijing 100049, China
[5] State Key laboratory for Plant Molecular Genetics, Center of Excellence for Molecular Plant Sciences, Chinese Academy of Sciences, Shanghai 200032, PR China

* Correspondence: Xinyou.Yin@wur.nl or cwzhu@issas.ac.cn

Received 17 July 2024; Editorial decision 15 April 2025; Accepted 27 May 2025

Editor: Robert Sharwood, Western Sydney University, Australia

Abstract

Photosynthesis under fluctuating irradiance is understudied, especially its response to elevated CO_2 and temperature in field environments. We measured photosynthesis after a single-step irradiance change and during a series of lightflecks for rice (*Oryza sativa* L.) grown under combinations of two CO_2 levels (ambient and elevated by 200 μmol mol^{-1}) and two temperature levels (ambient and increased by 2.0 °C) by temperature by free-air CO_2 enrichment systems in 2 years. The cumulative CO_2 fixation (CCF) during a single-step irradiance increase and during lightflecks was linearly correlated with final steady-state photosynthesis at the high irradiance (A_{nf}) under elevated CO_2 and temperature in both years. Across developmental stages, responses of CCF during a single-step irradiance increase and during lightflecks to elevated growth CO_2, to elevated growth temperature, to elevated measurement CO_2, and to elevated measurement temperature were all in the same magnitude as responses of A_{nf} to these variables. Lightfleck utilization efficiency (LfUE), defined as the ratio of CCF to assimilation expected from equivalent steady-state irradiance levels, showed a large variation among sequential lightflecks, and this was related to the variation of stomatal conductance (g_s) among the sequential lightflecks. Thus, steady-state photosynthesis models may not result in critical errors in predicting the effects of elevated CO_2 and temperature on dynamic photosynthesis provided that g_s in responses to fluctuating irradiance can be quantified reliably.

Keywords: Climate change, dynamic photosynthesis, elevated temperature, fluctuating irradiance, *Oryza sativa* L., stomatal conductance, T-FACE.

Introduction

Atmospheric CO_2 concentration and global mean surface air temperature are rising. It is likely that the CO_2 level will reach 500–1000 μmol mol^{-1} and air temperature will rise by 1.0–3.7 °C by 2100 (Ciais *et al.*, 2013). Much effort has been put into quantifying and understanding the responses of leaf photosynthesis in various crops to these climate change variables under steady-state conditions (Pozo *et al.*, 2005; Borjigidai *et al.*, 2006; Alonso *et al.*, 2009; Adachi *et al.*, 2014; Cai *et al.*, 2018). However, the field environment, in which crops grow, is almost never at a steady state. Of environmental variables, the incident irradiance (I_{inc}) on leaves of field-grown crops often changes rapidly as the sun, clouds, or leaves themselves move, causing dynamic photosynthesis (Pearcy, 1990; Smith and Berry, 2013; Kaiser *et al.*, 2017b; Faralli *et al.*, 2019). To predict C_3 crop performance under future climate conditions, it is important to understand how photosynthesis under fluctuating irradiance responds to elevated CO_2 and temperature.

Photosynthesis in leaves responds to both sudden rises and drops in irradiance, but these responses may not be symmetric (Chazdon and Pearcy, 1986a; Kaiser *et al.*, 2017b; Yamori *et al.*, 2020; Kang *et al.*, 2021). It can take photosynthesis between seconds and tens of minutes to reach a new steady state during the transition from one irradiance to another, causing loss of 10–40% of diurnal photosynthesis (Taylor and Long, 2017; Salter *et al.*, 2019; Acevedo-Siaca *et al.*, 2020; Long *et al.*, 2022). Both short- and long-term elevated CO_2 generally increase dynamic photosynthesis rates in C_3 plants beyond their effects on steady-state photosynthesis rates (Naumburg and Ellsworth, 2000; Leakey *et al.*, 2002; Tomimatsu *et al.*, 2014; Kaiser *et al.*, 2015, 2017b). The enhancement of dynamic photosynthesis rates by short- and long-term elevated CO_2 for C_3 plants is 5–17% (Leakey *et al.*, 2002; Kaiser *et al.*, 2015, 2017b). Short-term high-temperature inhibition of dynamic photosynthesis is greater than that of steady-state photosynthesis (Leakey *et al.*, 2003). Elevated CO_2 under future climate change is associated with elevated temperature. However, dynamic photosynthesis responses to combined elevated CO_2 and elevated temperature have not yet been quantified.

Of the studies on dynamic photosynthesis in response to elevated CO_2 or elevated temperature, those using field-grown plants in a FACE (free-air CO_2 enrichment) system to investigate dynamic photosynthesis responses are most relevant, because these plants in high-CO_2 treatments are exposed to natural diurnal and seasonal fluctuations in irradiance, temperature, and other environmental factors (Naumburg and Ellsworth, 2000; Leakey *et al.*, 2002). Recently, the FACE system was extended, by increasing temperature as well: T-FACE (Ruiz-Vera *et al.*, 2015; Cai *et al.*, 2016; Usui *et al.*, 2016). Previous T-FACE studies showed that a prolonged increase in CO_2 and temperature over the growing season caused strong acclimation of steady-state leaf photosynthesis (Adachi *et al.*, 2014; Cai *et al.*, 2018, 2020; Yuan *et al.*, 2021). However, dynamic photosynthesis in response to elevated CO_2 and elevated temperature in T-FACE environments is still unknown. Some studies found that dynamic photosynthesis was strongly correlated with steady-state photosynthesis (Ohkubo *et al.*, 2020; Taniyoshi *et al.*, 2020), while other studies found no significant correlations (Soleh *et al.*, 2017; Acevedo-Siaca *et al.*, 2020, 2021). Whether and how acclimation to long-term elevated CO_2 and temperature affect photosynthesis responses to fluctuating irradiance remain to be tested.

Response of dynamic photosynthesis has often been investigated by means of introducing a sudden increase or intermittent changes in incident irradiance. The response to a single sudden increase in incident irradiance is termed photosynthetic induction, while intermittent changes in incident irradiance are termed lightflecks. Reported mechanisms for the effects of elevated CO_2 or elevated temperature on dynamic photosynthetic induction are inconsistent (Leakey *et al.*, 2002, 2003; Tomimatsu and Tang, 2012; Kaiser *et al.*, 2017b). For example, Kaiser *et al.* (2017b) found that elevated CO_2 enhanced the response rate of photosynthesis during induction due to an increase in activation of Rubisco, while Tomimatsu and Tang (2012) suggested that the response rate of photosynthesis to elevated CO_2 during induction depended on the balance between a 'decrease' in maximum stomatal conductance and a 'decrease' in stomatal opening rate. Overall, according to Pearcy (1990) and Yamori (2016), physiological factors controlling photosynthetic induction and the responses to lightflecks can be mainly categorized into three processes: (i) induction of photosynthetic electron transport rates in the thylakoid membrane; (ii) Calvin cycle enzyme activities; and (iii) stomatal opening. In addition, induction kinetics of mesophyll conductance may also play a role (Liu *et al.*, 2022; Zeng *et al.*, 2024).

The objectives of this study were (i) to quantify responses of dynamic photosynthesis to long-term elevated CO_2 and temperature under field conditions, and (ii) to investigate which physiological process determines dynamic photosynthesis responses to elevated CO_2 and temperature. Previously, we found that elevated CO_2 and temperature strongly affected steady-state photosynthetic biochemistry and stomatal conductance for rice under T-FACE (Cai *et al.*, 2018, 2020). We hypothesized that (i) dynamic photosynthetic parameters would show strong acclimation to elevated growth CO_2 and growth temperature; (ii) the responses of integrated photosynthesis during fluctuating irradiance to elevated measurement CO_2, elevated growth CO_2, elevated measurement temperature, and elevated growth temperature were not correlated with those of steady-state photosynthesis; and (iii) both biochemical parameters and stomatal conductance controlled dynamic photosynthesis during photosynthetic induction and during lightflecks in response to elevated measurement CO_2, elevated growth CO_2, elevated measurement temperature, and elevated

Table 1. Summary of the environmental conditions in T-FACE experiments of 2021 and 2023

	2021 experiment	2023 experiment
CO_2 concentration increment relative to CT (μmol mol^{-1})		
C^+T	190 (38)	203 (20)
C^+T^+	183 (28)	203 (20)
Temperature increment relative to CT (°C)		
CT^+ Canopy temperature	2.2 (1.0)	1.8 (0.1)
Water temperature	–	2.2 (0.3)
C^+T^+ Canopy temperature	1.8 (0.5)	1.8 (0.2)
Water temperature	–	2.1 (0.2)
Mean daily air temperature for CT (°C)	26.6 (2.7)	25.6 (4.8)
Mean daily global radiation (MJ m^{-2} d^{-1})	13.8 (6.4)	13.2 (6.0)
N application		
Time of N application (day)[a]	0; 33; 53	1; 18; 56
Amount of N application (g m^{-2})[b]	6.9; 6.0; 5.2	9.6; 7.2; 7.2

CT, C^+T, CT^+, and C^+T^+ stand for ambient conditions, elevated CO_2, elevated temperature, and the combination of elevated CO_2 and elevated temperature, respectively.
'–' Water temperature was not elevated in the 2021 experiment (see the text).
Weather data in the table represent seasonal average values (SD between the daily values in parentheses).
[a] The time of N application is expressed in days after transplanting.
[b] N was all applied before the stem elongation stage and split into three applications (the first was the basal, followed by two top-dressing applications).

growth temperature. Photosynthesis during fluctuating irradiance was therefore measured on rice leaves under T-FACE. Addressing these questions will help to provide insights into, and have strong implications for modelling of, rice photosynthesis in future climatic environment in response to fluctuating irradiance.

Materials and methods

Experiment site, T-FACE set-up, and experimental treatments

We conducted field experiments in T-FACE for 2 years, 2021 and 2023. For both years, we sprayed pure CO_2 during the daytime and increased temperature during both the daytime and night-time. The set-up of T-FACE, however, differed somewhat between the years.

The T-FACE system used in the 2021 experiment is as described by Cai *et al.* (2016, 2018). Briefly, the T-FACE system was established at Kangbo village (31° 0′ N, 120°33′ E), Guli Township, Changshu Municipality, Jiangsu, China, in 2010. This experimental site represents a typical rice–wheat rotation system within a subtropical monsoon climatic zone. The target atmospheric CO_2 concentration under elevated CO_2 has been changed from 500 μmol mol^{-1} in the set-up described by Cai *et al.* (2016, 2018) to 590 μmol mol^{-1} in the present study. There were four CO_2 and temperature treatments in the T-FACE in 2021: (i) CT, where ambient conditions were maintained (control); (ii) C^+T, where the target atmospheric CO_2 was up to 590 μmol mol^{-1}; (iii) CT^+, where the canopy temperature was warmed by 2.0 °C; and (iv) C^+T^+, where CO_2 enrichment was combined with warming. Each treatment had three replicated plots.

The T-FACE system used in the 2023 experiment was newly established at Zhouzi village (31°53′ N, 119°4′ E), Jiangning District, Nanjing Municipality, Jiangsu, China, in 2023. This experimental site also represents a typical rice–wheat rotation system within a subtropical monsoon climatic zone. There were also four CO_2 and temperature treatments in 2023 but the set-up differed slightly from that of 2021: (i) CT, where ambient conditions were maintained (control); (ii) C^+T, where the target atmospheric CO_2 was 200 μmol mol^{-1} above the ambient conditions; (iii) CT^+, where both paddy water and canopy temperatures were warmed by 2.0 °C; and (iv) C^+T^+, where CO_2 enrichment was combined with warming. Water depth averaged 6 cm in the paddy field. Each treatment also had three replicated plots, and further information about the 2023 T-FACE set-up is shown in Supplementary Fig. S1.

Rice (*japonica* subspecies) cv. Wuyugeng 23 was chosen to grow in the 2 years. In the experiments in both years, seeds were sown at ambient air in late May, and three-leaf-stage seedlings were manually transplanted at a density of 24 hills m^{-2} (16.7 cm×25.0 cm in 2021, and 14.5 cm×28.9 cm in 2023), with two seedlings per hill, in all plots. The transplanting date was 25 June in 2021 and 30 June in 2023. Treatments with CO_2 enrichment started on 5 July and lasted until harvest in both years. Warming treatments also started on 5 July till harvest in 2021. However, in 2023, to avoid any effect of transplanting shock, warming treatments were started on July 25 and lasted essentially until harvest. To follow the local agronomic practice of 'paddy soil drying' that is believed to remove non-productive tillers, water warming was no longer relevant, and thus was stopped for 10 d prior to the harvest (14–24 October), while the elevated canopy-warming treatment was still maintained. Daily weather data for maximal and minimal air temperatures, global radiation, relative humidity, wind speed, and precipitation during the growing season for both experiments under ambient conditions were recorded by local weather stations, and are shown in Supplementary Fig. S2. Average global radiation and realized average increases in CO_2 concentration and in temperature in both years are summarized in Table 1.

Gas exchange measurements

Leaf-level gas exchange measurements were conducted using the Li-Cor 6400XT portable photosynthesis system (Li-Cor Bioscience, Lincoln, NE, USA) equipped with an LED head (2×3 LED, LI-6400-02B), at the stem elongation stage, the flowering stage, and the grain-filling stage (22 d after flowering) in the 2021 experiment. In the 2023 experiment, gas exchange measurements were conducted at the flowering stage and the grain-filling stage (18 d after flowering). Detailed information about leaf temperatures (T_{leaf}) and CO_2 levels (C_a) in the leaf chamber used for measurements is shown in Table 2. In both experiments, measurements were replicated using the three youngest fully expanded leaves at each stage and in each treatment, one from each of the three replicated plots. During

Table 2. Leaf temperatures (T_{leaf}) and CO_2 levels (C_a) used for measuring induction curves and lightflecks during various developmental stages under ambient conditions (CT), elevated CO_2 (C^+T), elevated temperature (CT^+), and the combination of elevated CO_2 and elevated temperature (C^+T^+) in the 2021 and 2023 experiments for rice

		2021		2023	
		T_{leaf} (°C)	C_a (μmol mol^{-1})	T_{leaf} (°C)	C_a (μmol mol^{-1})
Induction curve	A single-step irradiance increase	33	100, 200, 300, 390, 590, and 800	33	400 and 600
				31	100, 200, 300, 400, 600, 800, 1000, 1200, and 1500
	A single-step irradiance decrease	33	390 (CT and CT^+) and 590 (C^+T and C^+T^+)	33	400 and 600
				31	400 and 600
Lightflecks	1 min-HL-lightflecks	33	390 (CT and CT^+) and 590 (C^+T and C^+T^+)	33	400 and 600
				31	400 and 600
	3 min-HL-lightflecks	33	390 (CT and CT^+) and 590 (C^+T and C^+T^+)		
	1 min-LH-lightfkecks			33	400 and 600
				31	400 and 600

A single-step irradiance increase is a one-step irradiance increase from 50 μmol m^{-2} s^{-1} to 1500 μmol m^{-2} s^{-1}; a single-step irradiance decrease is a one-step irradiance decrease from 1500 μmol m^{-2} s^{-1} to 50 μmol m^{-2} s^{-1}; 1 min-HL-lightflecks are nine repeated cycles of 1 min of I_{inc} (incident irradiance) of 1500 μmol m^{-2} s^{-1}(high irradiance) followed by 1 min of I_{inc} of 50 μmol m^{-2} s^{-1} (low irradiance); 3 min-HL-lightflecks are three repeated cycles of 3 min of I_{inc} of 1500 μmol m^{-2} s^{-1} followed by 3 min of I_{inc} of 50 μmol m^{-2} s^{-1}; 1 min-LH-lighflecks are nine repeated cycles of 1 min of I_{inc} of 50 μmol m^{-2} s^{-1} followed by 1 min of I_{inc} of 1500 μmol m^{-2} s^{-1} (see the text).

the measurements, leaf-to-air vapour pressure difference was maintained between 0.5 kPa and 2.0 kPa, and the flow rate was 500 μmol s^{-1}. All the measurements were logged every 5 s.

In the 2021 experiment, for measuring the induction curves, leaves were adapted to incident irradiance (I_{inc}) of 50 μmol m^{-2} s^{-1} for 30 min prior to starting gas exchange measurements. Then I_{inc} was switched to 1500 μmol m^{-2} s^{-1} and stayed at this light level for 15 min for photosynthesis and stomatal conductance to reach steady-state values. Finally, I_{inc} was switched back to 50 μmol m^{-2} s^{-1} for 20 min. To further investigate the dynamic behaviour of photosynthesis and stomatal conductance but in response to intermittent changes in irradiance, leaves were also adapted to I_{inc} of 50 μmol m^{-2} s^{-1} for 30 min and then subjected to two sets of lightflecks. The first set consisted of nine repeated cycles of 1 min of high I_{inc} of 1500 μmol m^{-2} s^{-1} followed by 1 min of low I_{inc} of 50 μmol m^{-2} s^{-1} (1 min-HL-lightflecks). The second set consisted of three repeated cycles of 3 min of 1500 μmol m^{-2} s^{-1} followed by 3 min of 50 μmol m^{-2} s^{-1} (3 min-HL-lightflecks). The total measurement time lasted for 18 min (1080 s) for each set of lightflecks. For induction curves in response to a single-step I_{inc} increase, the C_a levels were kept at both 390 μmol mol^{-1} and 590 μmol mol^{-1} for all treatments. However, for measuring the responses to a single-step I_{inc} decrease and to lightflecks, the C_a level was kept at the respective growth [CO_2] level, namely 390 μmol mol^{-1} for CT and CT^+ treatments, and 590 μmol mol^{-1} for C^+T and C^+T^+ treatments. All these curves were measured at a T_{leaf} of 33 °C.

In the 2023 experiment, the measurement protocol differed somewhat from the 2021 experiment (Table 2). For all treatments, the induction curves by one-step irradiance change (including an increase and decrease) were measured at four combinations of two C_a levels (400 μmol mol^{-1} and 600 μmol mol^{-1}) and two T_{leaf} levels (31 °C and 33 °C). Responses to intermittent changes in irradiance were measured with two sets of lightflecks. The first set was 1 min-HL-lightflecks, the same as in the 2021 experiment, with leaves initially adapted at 50 μmol m^{-2} s^{-1} for 30 min prior to measurements. As leaves of field-grown crops are also exposed to high irradiance and suddenly experience rapid changes between low and high irradiance (Yamori *et al.*, 2020), for the second set, we reversed the order of the lightflecks (i.e. nine repeated cycles of 1 min of I_{inc} of 50 μmol m^{-2} s^{-1} followed by 1 min of I_{inc} of 1500 μmol m^{-2} s^{-1}), with leaves initially adapted at 1500 μmol m^{-2} s^{-1} for 30 min prior to measurements. To distinguish it from the first 1 min-HL-lightflecks set, we named the second set 1 min-LH-lightflecks. Both sets for each treatment were measured at four combinations of two C_a levels (400 μmol mol^{-1} and 600 μmol mol^{-1}) and two T_{leaf} levels (31 °C and 33 °C).

To calculate biochemical parameters J (the rate of linear electron transport, μmol m^{-2}–s^{-1}) and V_{cmax} (the maximum rate of carboxylation by Rubisco, μmol m^{-2} s^{-1}) during induction, additional induction curves in response to a single-step irradiance increase were measured for all treatments according to Soleh *et al.* (2016). In the 2021 experiment, these induction curves were made with six C_a levels (100, 200, 300, 390, 590, and 800 μmol mol^{-1}) at a T_{leaf} of 33 °C so that photosynthetic CO_2 response curves could be constructed. These constructed curves were used to fit a biochemical model to estimate J and V_{cmax} for various time points of induction (see later). Following the 2021 experiment, the 2023 measurement protocol was adjusted somewhat (Table 2). First, to improve estimations of J and V_{cmax}, photosynthetic CO_2 response curves were constructed with nine C_a levels (100, 200, 300, 400, 600, 800, 1000, 1200, and 1500 μmol mol^{-1}). Second, steady-state light response curves at the strictly limiting level (I_{inc} <200 μmol m^{-2} s^{-1}) were measured at a T_{leaf} of 31 °C for all treatments to provide data for better estimating R_d (day respiration) (Yin and Amthor, 2024). For measuring steady-state light response curve, leaves were first adapted to an I_{inc} of 200 μmol m^{-2} s^{-1} for at least 10 min prior to starting gas exchange measurements. Then I_{inc} was decreased in the order of 200, 150, 100, 50, and 20 μmol m^{-2} s^{-1} (5 min per I_{inc} step), while keemnbdsq ping C_a at 400 μmol mol s^{-1}.

Estimation of photosynthetic parameters during a single-step change in irradiance

The photosynthetic induction state was calculated as transient A_n (net photosynthesis rate) as a percentage of the final steady-state A_n (A_{nf}), corrected for the initial value (A_{ni}):

$$Photosynthetic\ induction\ (\%) = \frac{A_n - A_{ni}}{A_{nf} - A_{ni}} \times 100 \quad (1)$$

where A_{ni} is the steady-state A_n at an initial I_{inc} of 50 μmol m^{-2} s^{-1}, and A_{nf} is the steady-state A_n at a final I_{inc} of 1500 μmol m^{-2} s^{-1}. For the induction curves, the times required to reach 50% ($IT_{50,A}$) and 90% ($IT_{90,A}$)

of full photosynthetic induction were calculated. We checked whether the values of $IT_{50,A}$ (s) and $IT_{90,A}$ (s) correlated with initial steady-state stomatal conductance (g_{si}), given the previous reports on their correlations (Allen and Pearcy, 2000a, b; Naumburg and Ellsworth, 2000; Kaiser *et al.*, 2016). The value of g_{si} was taken as stomatal conductance at an I_{inc} of 50 μmol m^{-2} s^{-1} at initiating induction. In addition, we also checked if they were related to the final steady-state stomatal conductance at an I_{inc} of 1500 m^{-2} s^{-1} (g_{sf}).

From induction curves, we calculated: (i) $CCF_{I\text{-}600s}$ [in mmol m^{-2} (600 s)$^{-1}$], the cumulative CO_2 fixation (CCF) in the first 600 s after the increase in irradiance; and (ii) $CCF_{D\text{-}60s}$ [in mmol m^{-2} (60 s)$^{-1}$], the cumulative CO_2 fixation in the first 60 s after the decrease in irradiance. The values of 600 s and 60 s were chosen because A_n hardly changed beyond these time points (see the Results).

The measurement of the induction response at different CO_2 concentrations generated the responses of A_n to C_i (intercellular CO_2 concentration) at different time points during induction. This allowed estimation of the biochemical parameters J and V_{cmax} for different times during induction (Soleh *et al.*, 2016). V_{cmax} and J were calculated based on the C_3 photosynthesis model of Farquhar *et al.* (1980; the FvCB model; see Supplementary Protocol S1 for the model equations). With the estimated J and V_{cmax} during induction, the time for 50% and 90% induction of V_{cmax} ($IT_{50,Vcmax}$, $IT_{90,Vcmax}$) and of J ($IT_{50,J}$, $IT_{90,J}$) were calculated.

Our data of the induction responses allowed us to separate the effect of growth versus measurement conditions on parameter values. For the 2021 experiment, we were able to separate the effect of growth versus measurement CO_2 on many parameters. Values of A_{ni}, A_{nf}, $IT_{50,A}$, $IT_{90,A}$, g_{si}, g_{sf}, and $CCF_{I\text{-}600s}$ were estimated at measurement CO_2 levels of both 390 μmol mol^{-1} and 590 μmol mol^{-1} for all treatments, allowing investigation of whether these photosynthetic parameters acclimated to elevated growth CO_2 and growth temperature (see the Results). However, we were not able to do this for $CCF_{D\text{-}60s}$, because we did not measure curves after a single-step irradiance decrease at 590 μmol mol^{-1} for CT and CT^+ treatments and at 390 μmol mol^{-1} for C^+T and C^+T^+ treatments. For the 2023 experiment, the data of the induction response at four measurement combinations of two C_a levels (400 μmol mol^{-1} and 600 μmol mol^{-1}) and two T_{leaf} levels (31 °C and 33 °C) for each treatment allowed us to (i) separate the effects of growth CO_2, measurement CO_2, growth temperature, and measurement temperature on photosynthetic parameters; and (ii) investigate whether photosynthetic parameters acclimated to elevated growth CO_2 and growth temperature (see the Results).

Estimation of photosynthetic parameters during lightflecks

For lightflecks, the photosynthetic induction state was also calculated using Equation 1, according to Leakey *et al.* (2003), where A_{nf} and A_{ni} were steady-state A_n at an I_{inc} of 1500 μmol m^{-2} s^{-1} and 50 μmol m^{-2} s^{-1}, respectively, taken from the aforementioned photosynthetic induction curves measured on the same leaves in the same treatment and developmental stage. Values of $IT_{50,A}$ and $IT_{90,A}$ after exposure to high irradiance in each single 1 min-HL-lightfleck, 3 min-HL-lightfleck, or 1 min-LH-lightfleck were then estimated. We also checked whether the photosynthetic induction rate correlated with stomatal conductance in each lightfleck. However, as stomatal conductance in each lightfleck did not reach a steady-state value, we defined g_{si} and g_{sf} as stomatal conductance at the onset and at the end, respectively, of high irradiance in each lightfleck, on the basis that there was no significant difference in photosynthetic induction rate in relation to g_{si} between a single-step irradiance increase and each lightfleck (see Results).

The cumulative CO_2 fixation during the 1080 s of 1 min-HL-lightflecks ($CCF_{L\text{-}1min\text{-}HL}$), of 3 min-HL-lightflecks ($CCF_{L\text{-}3min\text{-}HL}$), and of 1 min-LH-lighflecks ($CCF_{L\text{-}1min\text{-}LH}$), all in mmol m^{-2} (1080 s)$^{-1}$, were calculated by summing up the recorded instantaneous A_n during the periods. To analyse the effects of lightflecks on the photosynthetic carbon gain, the lightfleck utilization efficiency (LfUE, %) for single lightflecks was calculated as the ratio of CCF to assimilation expected from equivalent steady-state irradiance levels, following Chazdon and Pearcy (1986b; see also Supplementary Fig. S3). LfUE values were estimated for each lightfleck in the series as well as for the overall value of all lightflecks.

Statistical analyses

Constructed CO_2 response curves were analysed to estimate V_{cmax} and J with the GAUSS method in PROC NLIN of SAS (SAS Institute Inc, Cary, NC, USA). Prior to conducting statistical tests, normality and homogeneity of variances were tested using Shapiro–Wilk and Levene's test, respectively. If data were not normally distributed or not homogeneous, log transformation was performed. ANOVA was used to determine differences between treatments for all parameters described above. Linear regression was performed using Microsoft Excel. All results reported as significant had a P-value <0.05.

Results

Photosynthesis after a single-step change in irradiance

After a single-step irradiance increase from 50 μmol m^{-2} s^{-1} to 1500 μmol m^{-2} s^{-1}, photosynthesis and g_s for the four CO_2 and temperature treatments gradually increased in the experiments in both years (Supplementary Figs S4–S6). Photosynthesis and g_s reached steady-state after 600 s (10 min) of induction in all treatments at all growth stages in both experiments (Supplementary Figs S4–S6). With the subsequent single-step irradiance decrease from 1500 μmol m^{-2} s^{-1} to 50 μmol m^{-2} s^{-1}, photosynthesis dropped below A_{ni} within 30 s, but g_s dropped more slowly in all cases (Supplementary Figs S4–S6).

Dynamic photosynthetic parameters in both experiments were estimated using data of these induction curves and are shown in Supplementary Tables S1–S4. Data in Supplementary Tables S1–S4 allow us to correlate these parameters (CCF, $IT_{50,A}$, and $IT_{90,A}$) with those typical for steady-state photosynthesis (A_{nf} and A_{ni}). In the 2023 experiment, $CCF_{I\text{-}600s}$ and $CCF_{D\text{-}60s}$ were more significantly correlated with A_{nf} than with A_{ni} in all treatments (Fig. 1). The linear relationships between $CCF_{I\text{-}600s}$ (or $CCF_{D\text{-}60s}$) and A_{ni} was significantly altered by elevated CO_2 treatments (C^+T and/or C^+T^+) (Fig. 1A, C). The photosynthetic induction parameter $IT_{90,A}$ was weakly (but significantly) correlated with A_{nf} under CT and CT^+, and this relationship significantly differed between the two treatments (Supplementary Fig. S7D). The relationship between $CCF_{I\text{-}600s}$ or $CCF_{D\text{-}60s}$ and A_{nf} in the 2021 experiment (Supplementary Fig. S8) was almost the same as that in the 2023 experiment. However, $IT_{50,A}$ and $IT_{90,A}$ in 2021 had no significant relationship with A_{ni}, or with A_{nf} (Supplementary Fig. S8E–H).

Quantitative analysis using data from Supplementary Tables S1–S4 showed that in the 2023 experiment, elevated measurement CO_2 increased $CCF_{D\text{-}60s}$, $CCF_{I\text{-}600s}$, and A_{nf} by 33–37% and A_{ni} by 28%, but decreased g_{sf}, g_{si}, and $IT_{90,A}$ by 17–35% and $IT_{50,A}$ by 7% (Fig. 2; Supplementary Fig. S9). Elevated growth CO_2 decreased $CCF_{D\text{-}60s}$ by 1%, $CCF_{I\text{-}600s}$, A_{ni}, and

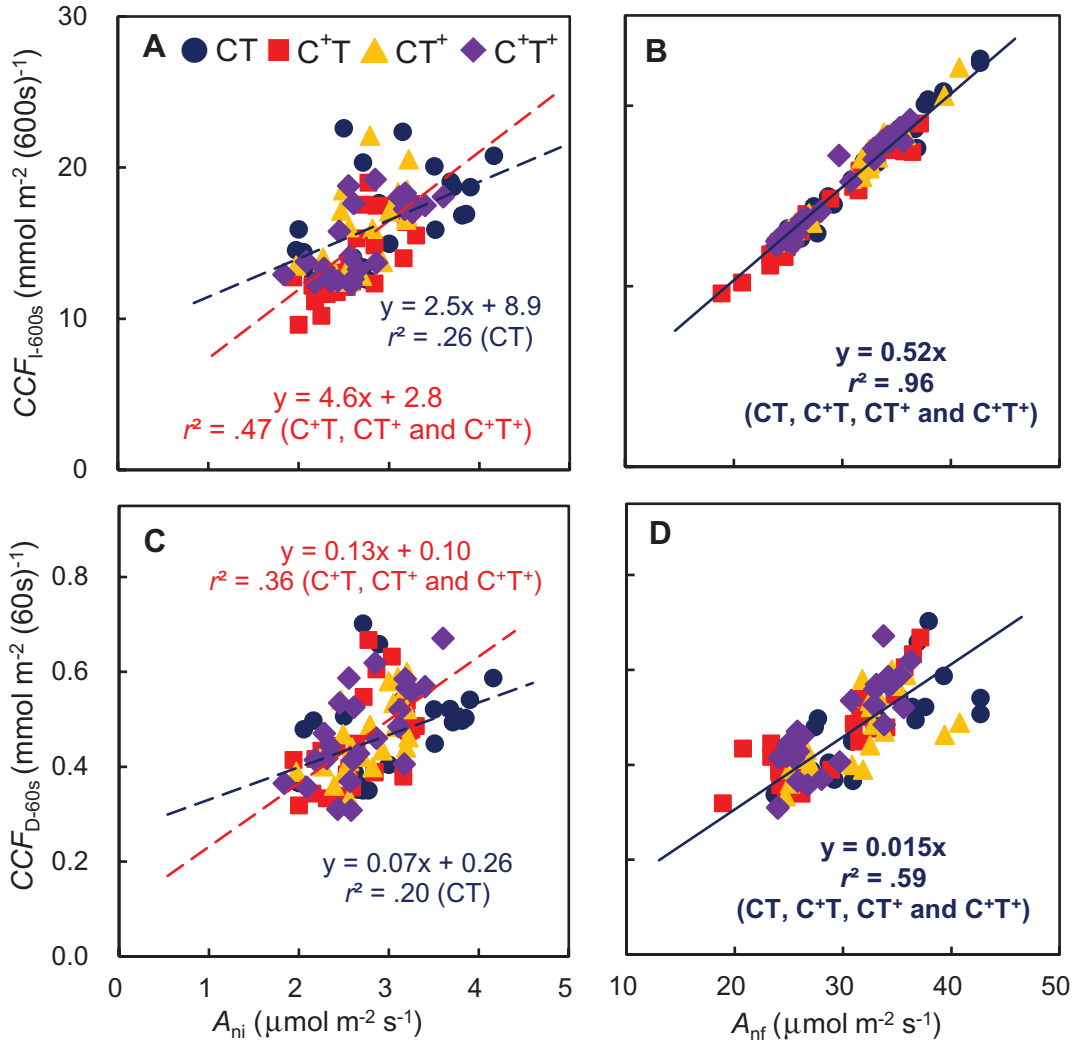

Fig. 1. Relationships between CCF and A_{ni} or A_{nf} during a single-step change in irradiance in the 2023 experiment. Relationships between CCF and A_{ni} or A_{nf} during a single-step change in irradiance under ambient conditions (circles, CT), elevated CO_2 (squares, C^+T), elevated temperature (triangles, CT^+), and the combination of elevated CO_2 and elevated temperature (diamonds, C^+T^+) in the 2023 experiment. $CCF_{I\text{-}600s}$ is the cumulative CO_2 fixation (CCF) in the first 600 s after the increase in irradiance; $CCF_{D\text{-}60s}$ is the CCF in the first 60 s after the decrease in irradiance; A_{ni} is the initial steady-state net photosynthetic rate (A_n) at I_{inc} (incident irradiance) of 50 µmol m^{-2} s^{-1}; and A_{nf} is the final steady-state A_n at I_{inc} of 1500 µmol m^{-2} s^{-1}. Statistical parameters given in the panels are in bold if the relationship was shared for the four treatments. The lines represent significant linear regressions (P<0.05).

A_{nf} by 6–9%, and g_{si} and g_{sf} by 18–27%, but increased $IT_{50,A}$ and $IT_{90,A}$ by 5–13% (Fig. 2; Supplementary Fig. S9). Overall, the effects of elevated measurement temperature and growth temperature were marginal (Fig. 2; Supplementary Fig. S9). Elevated measurement temperature decreased $CCF_{D\text{-}60s}$, A_{ni}, g_{sf},g_{si}, $IT_{50,A}$, and $IT_{90,A}$ by 1–6%, but increased $CCF_{I\text{-}600s}$ by 1% and did not affect A_{nf} (Fig. 2; Supplementary Fig. S9). Elevated growth temperature decreased A_{ni} and A_{nf} by 1–4% and g_{si}, $IT_{50,A}$, and $IT_{90,A}$ by 9–15%, but increased $CCF_{D\text{-}60s}$, $CCF_{I\text{-}600s}$, and g_{sf} by 1–2% (Fig. 2; Supplementary Fig. S9). In the 2021 experiment, the effects of elevated measurement CO_2, elevated growth CO_2, and elevated growth temperature on these photosynthetic parameters were generally similar to those from the 2023 experiment (Fig. 2; Supplementary Figs S9, S10). All these results in both experiments indicated that the effects of measurement CO_2, growth CO_2, measurement temperature, and growth temperature on CCF during a single-step change in irradiance were of almost the same extent as their effects on A_{nf} (Fig. 2; Supplementary Figs S9, S10).

Biochemical parameters and their relationships with photosynthesis during induction

In the 2023 experiment, there were no significant effects of elevated growth CO_2, elevated growth temperature, and their interaction on $IT_{50,Vcmax}$, $IT_{90,Vcmax}$, $IT_{50,J}$, and $IT_{90,J}$ at

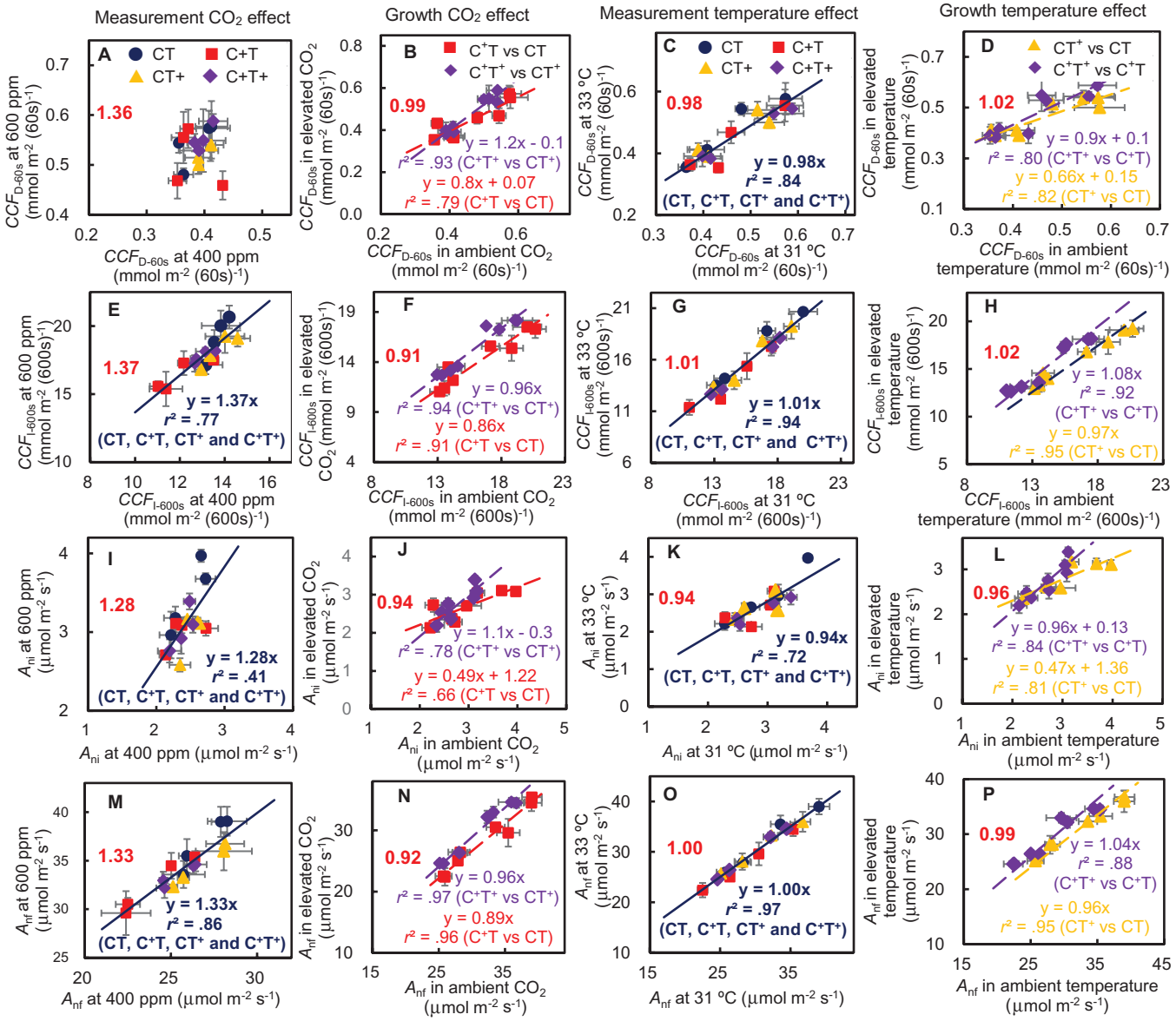

Fig. 2. Effects of measurement CO_2, growth CO_2, measurement temperature, and growth temperature on $CCF_{D\text{-}60s}$, $CCF_{I\text{-}600s}$, A_{ni}, and A_{nf} in the 2023 experiment. Effects of measurement CO_2 (the first column), growth CO_2 (the second column), measurement temperature (the third column), and growth temperature (the fourth column) on $CCF_{D\text{-}60s}$ (A–D), $CCF_{I\text{-}600s}$ (E–H), A_{ni} (I–L), and A_{nf} (M–P) during a single-step change in irradiance in the 2023 experiment. $CCF_{D\text{-}60s}$ is the cumulative CO_2 fixation (CCF) in the first 60 s after the decrease in irradiance; $CCFI_{\text{-}600s}$ is the CCF in the first 600 s after the increase in irradiance; A_{ni} is the initial steady-state net photosynthetic rate (A_n) at I_{inc} (incident irradiance) of 50 µmol m^{-2} s^{-1}; and A_{nf} is the final steady-state A_n at I_{inc} of 1500 µmol m^{-2} s^{-1}. Each data point is the mean value ±SE of three replications. Statistical parameters given in the panels are in bold if the lines were fitted for all data. The lines represent significant linear regressions (P<0.05). The bold number in red in each panel is the average ratio of y-axis to x-axis values.

all developmental stages (Supplementary Table S5). In the 2021 experiment, $IT_{90,Vcmax}$ was only significantly decreased by elevated growth temperature at the flowering stage (Supplementary Table S6). Significant interaction between growth CO_2 and growth temperature effects on $IT_{50,J}$ and $IT_{90,J}$ was observed for the stem elongation stage in 2021 (Supplementary Table S6).

Regression analysis showed that photosynthetic induction rates were weakly correlated with the induction rates of biochemical parameters in both experiments (Supplementary Figs S11, S12). In the 2023 experiment, the estimated $IT_{50,A}$ was significantly correlated with $IT_{50,J}$, and $IT_{90,A}$ was significantly correlated with $IT_{90,Vcmax}$, for C^+T at a measurement CO_2 level of 400 µmol mol^{-1} (Supplementary Fig. S11B, C). In the 2021

experiment, $IT_{50,A}$ was marginally correlated with $IT_{50,Vcmax}$ under CT at two measurement CO_2 levels (390 μmol mol^{-1} and 590 μmol mol^{-1}) and under C^+T and C^+T^+ at a measurement CO_2 level of 590 μmol mol^{-1} (Supplementary Fig. S12A). Furthermore, $IT_{50,A}$ was marginally correlated with $IT_{50,J}$ under CT and CT^+ at a measurement CO_2 level of 590 μmol mol^{-1} (Supplementary Fig. S12B). $IT_{90,A}$ was only significantly correlated with $IT_{90,Vcmax}$ under C^+T^+ at the two measurement CO_2 levels (Supplementary Fig. S12C).

Photosynthesis during lightflecks

In the 2023 experiment, the responses of photosynthetic rate and stomatal conductance to a series of 1 min-LH-lightflecks were notably different from those to a series of 1 min-HL-lightflecks (Supplementary Figs S13–S16). The LfUE of 1 min-HL-lightflecks increased gradually depending on the number within the lightfleck series (Fig. 3; Supplementary Fig. S17). However, LfUE of 1 min-LH-lightflecks slightly decreased depending on the number within the lightfleck series (Fig. 3; Supplementary Fig. S17). The 1080 s overall LfUE of the 1 min-LH-lightflecks was higher than that of the 1 min-HL-lightflecks in all treatments at all developmental stages (Fig. 3; Supplementary Fig. S17; Supplementary Table S7). In the 2021 experiment, the responses of photosynthetic rate and stomatal conductance to a series of 1 min-HL-lightflecks were generally similar to those to a series of 3 min-HL-lightflecks (Supplementary Figs S18, S19). Furthermore, the change of LfUE of 1 min-HL-lightflecks depending on the number within the lightfleck series was similar to that in the 2023 experiment (Fig. 3; Supplementary Figs S17, S20). The 1080 s overall LfUE of the 1 min-HL-lightflecks was higher than that of the 3 min-HL-lightflecks in all treatments at all developmental stages (Supplementary Table S8).

In the 2023 experiment, CCFs for 1080 s of 1 min-LH-lightflecks ($CCF_{L\text{-}1min\text{-}LH}$) and 1 min-HL-lightflecks ($CCF_{L\text{-}1min\text{-}HL}$) were more significantly correlated with A_{nf} than with A_{ni} in all treatments (Fig. 4). $LfUE_{1min\text{-}HL}$ or $LfUE_{1min\text{-}LH}$ in each lightfleck was more significantly correlated with g_{si} (Fig. 5A, C) than with g_{sf} (Fig. 5B, D) in all treatments. $LfUE_{1min\text{-}HL}$ and $LfUE_{1min\text{-}LH}$ increased linearly with an increase in g_{si} up to g_{si}, being ~0.29 mol m^{-2} s^{-1} at 400 ppm and ~0.24 mol m^{-2} s^{-1} at 600 ppm, beyond which $LfUE_{1min\text{-}HL}$ and $LfUE_{1min\text{-}LH}$ did not vary further with increasing g_{si} (Fig. 5A, C). There also appeared to be a threshold g_{sf} for $LfUE_{1min\text{-}HL}$ and $LfUE_{1min\text{-}LH}$ in each lightfleck at 400 μmol mol^{-1} (~0.50 mol m^{-2} s^{-1}, Fig. 5B) and at 600 μmol mol^{-1} (~0.39 mol m^{-2} s^{-1}, Fig. 5D). In addition, we observed threshold g_{si} for $IT_{50,A}$ at 400 μmol mol^{-1} (~0.24 mol m^{-2} s^{-1}, Fig. 6A) and at 600 μmol mol^{-1} (~0.19 mol m^{-2} s^{-1}, Fig. 6B) and for $IT_{90,A}$ at 400 μmol mol^{-1} (~0.29 mol m^{-2} s^{-1}, Fig. 6E) and at 600 μmol mol^{-1} (~0.22 mol m^{-2} s^{-1}, Fig. 6F). These relationships were not affected by elevated CO_2 and temperature (Figs 4–6). In the 2021 experiment, the relationships between $CCF_{L\text{-}1min\text{-}HL}$ and A_{nf} or A_{ni} and between $IT_{50,A}$ and g_{si} were similar to those from the 2023 experiment (Supplementary Figs S21, S22). The relationships between CCF and A_{nf} or A_{ni}, and between LfUE and g_{si} for 1 min-HL-lightflecks were generally similar to those for 3 min-HL-lightflecks in the 2021 experiment (Supplementary Figs S21, S23).

In the 2023 experiment, elevated measurement CO_2 significantly increased $CCF_{L\text{-}1min\text{-}HL}$ and $CCF_{L\text{-}1min\text{-}LH}$ during a series of lightflecks by 31–32%, but hardly affected $LfUE_{1min\text{-}HL}$ and $LfUE_{1min\text{-}LH}$ (Fig. 7; Supplementary Tables S7, S9). Elevated growth CO_2 significantly decreased $CCF_{L\text{-}1min\text{-}HL}$ and $CCF_{L\text{-}1min\text{-}LH}$ by 8–10%, but hardly affected $LfUE_{1min\text{-}HL}$ and $LfUE_{1min\text{-}LH}$ (Fig. 7; Supplementary Tables S7, S9). The elevated measurement temperature and growth temperature marginally affected CCF_L and LfUE during a series of lightflecks (Fig. 7). In the 2021 experiment, the effects of elevated growth temperature on CCF_L and LfUE during a series of lightflecks were also marginal and similar to those from the 2023 experiment (Supplementary Fig. S24). Overall, these effects on CCF during lightflecks were also similar in magnitude to the effect of measurement CO_2, of growth CO_2, of measurement temperature, and of growth temperature on steady-state photosynthesis A_{nf} in both experiments (Fig. 7; Supplementary Fig. S24).

Discussion

Current crop models integrated with steady-state photosynthetic models have been widely used to quantitatively assess the impacts of elevated CO_2 and temperature on crop growth and yield in the field (Yin, 2013; Hasegawa *et al.*, 2017; Wang *et al.*, 2021). However, incoming irradiance fluctuates continuously under field conditions, causing dynamic photosynthesis. Therefore, it is particularly important to investigate whether the effects of elevated CO_2 and temperature on dynamic photosynthesis can be accurately predicted by steady-state models. To address this issue, we investigated dynamic photosynthesis during a single-step change in irradiance and a series of lightflecks during the whole growth cycle under future climate conditions of (combined) elevated CO_2 and temperature as mimicked in T-FACE environments. In addition, our measurement protocol allowed us to separate the effects of growth CO_2 (or temperature) from measurement CO_2 (or temperature) on dynamic photosynthetic parameters.

Dynamic photosynthesis under ambient conditions

Most studies investigating dynamic photosynthesis of C_3 crops were conducted under ambient conditions, by assessing photosynthetic response to a single-step irradiance increase at a vegetative growth stage (Soleh *et al.*, 2016, 2017; Acevedo-Siaca *et al.*, 2020) or at a reproductive stage (Salter *et al.*, 2019; Acevedo-Siaca *et al.*, 2021). Their main findings were that (i) the slow rate of photosynthetic induction reduced >15% of potential assimilation (Salter *et al.*, 2019; Acevedo-Siaca *et al.*,

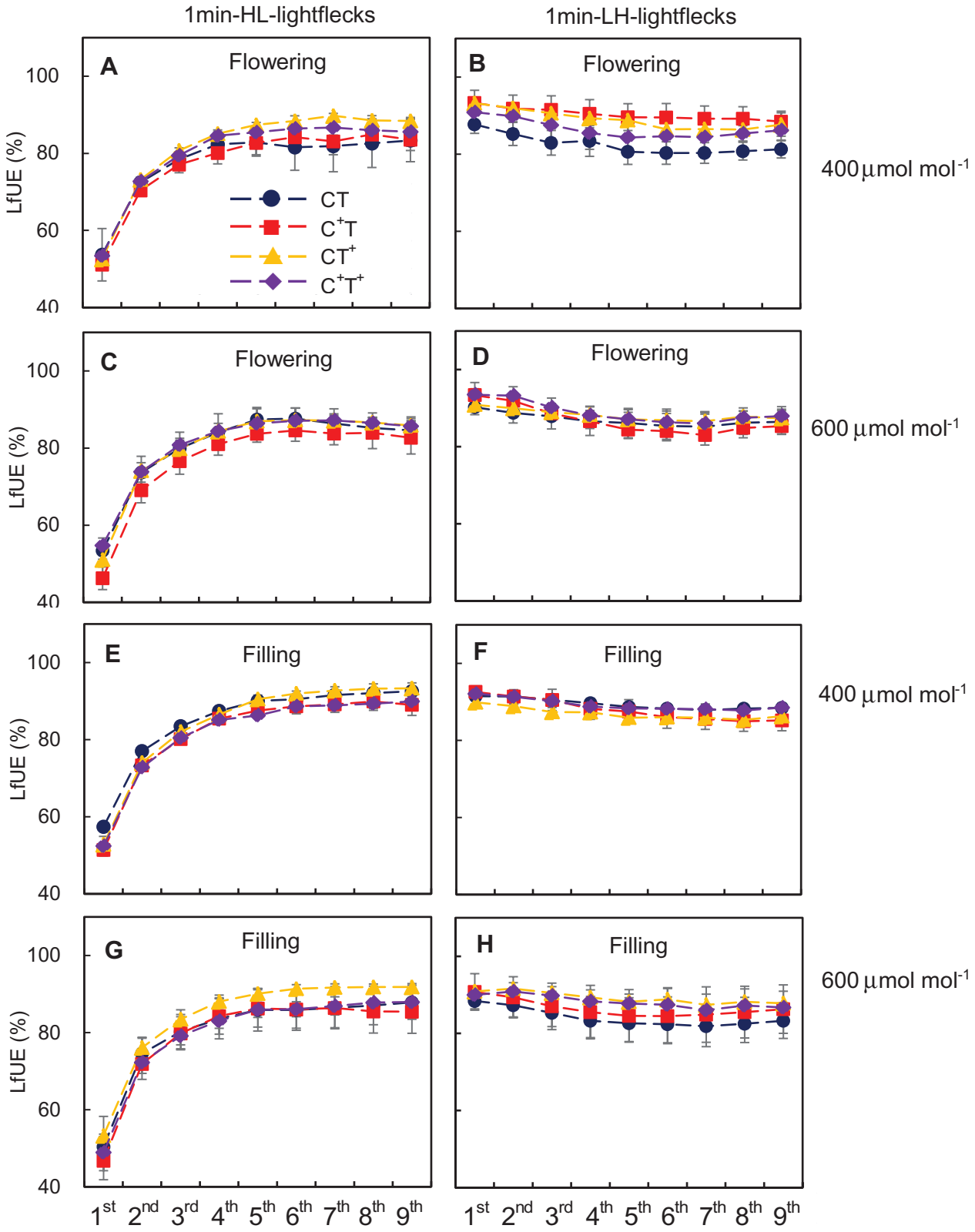

Fig. 3. Rice LfUE during the first to ninth 1 min-HL-lightflecks and during the first to ninth 1 min-LH-lightflecks in the 2023 experiment. Rice LfUE during the first to ninth 1 min-HL-lightflecks (A, C, E, G) and during the first to ninth 1 min-LH-lightflecks (B, D, F, H) for ambient conditions (circles, CT), elevated CO_2 (squares, C^+T), elevated temperature (triangles, CT^+), and the combination of elevated CO_2 and elevated temperature (diamonds, C^+T^+) at the flowering stage (A–D) and the grain-filling stage (E–H) in the 2023 experiment. LfUE is lightfleck utilization efficiency. A 1 min-HL-lightfleck is 1 min of I_{inc} (incident irradiance) of 1500 µmol m^{-2} s^{-1} (high irradiance) followed by 1 min of I_{inc} of 50 µmol m^{-2} s^{-1} (low irradiance), on leaves initially adapted at 50 µmol m^{-2} s^{-1} for 30 min prior to measurements. A 1 min-LH-lighfleck is 1 min of I_{inc} of 50 µmol m^{-2} s^{-1} followed by 1 min of I_{inc} of 1500 µmol m^{-2} s^{-1}, on leaves initially adapted at 1500 µmol m^{-2} s^{-1} for 30 min prior to measurements. LfUE for all treatments were estimated at measurement CO_2 levels of 400 µmol mol^{-1} and 600 µmol mol^{-1} (as indicated at the right side of the figure) and at measurement leaf temperature of 31 °C. Each data point is the mean value ±SE of three replications.

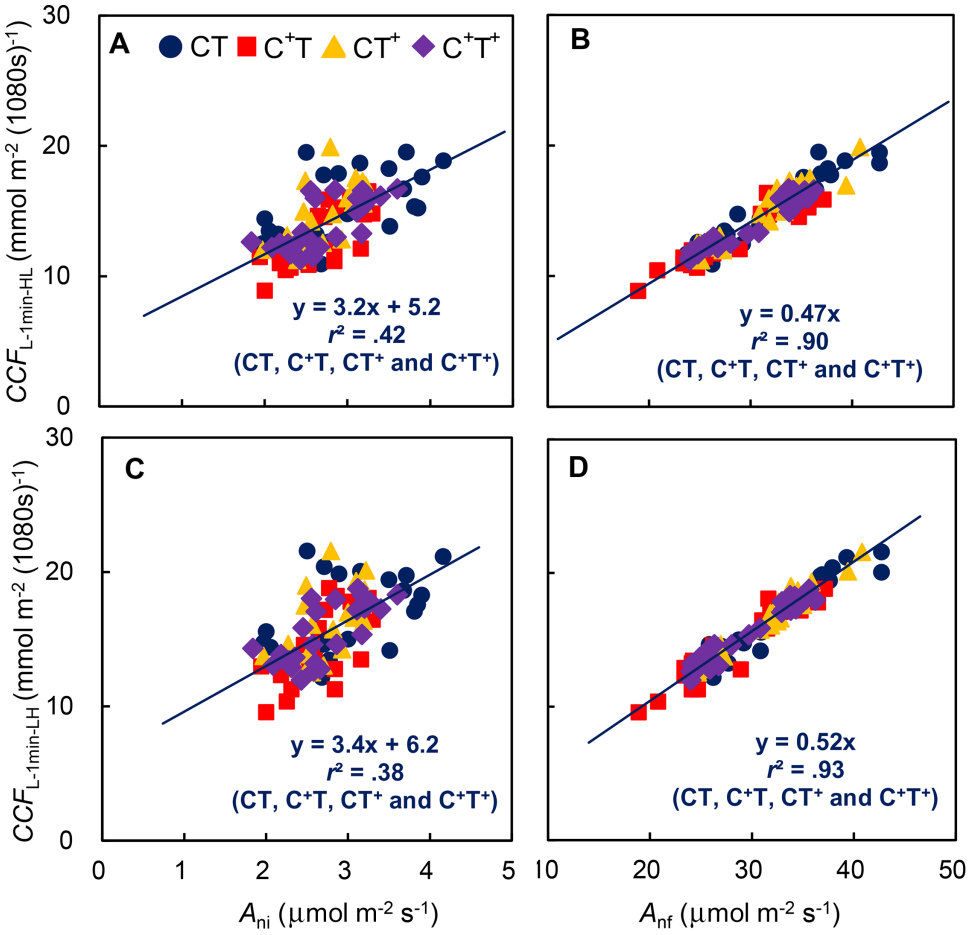

Fig. 4. Relationships between CCF during a series of lightflecks and A_{nf} or A_{ni} in the 2023 experiment. Relationships between CCF during a series of lightflecks and A_{nf} or A_{ni} for ambient conditions (circles, CT), elevated CO_2 (squares, C^+T), elevated temperature (triangles, CT^+), and the combination of elevated CO_2 and elevated temperature (diamonds, C^+T^+) at all stages in the 2023 experiment. $CCF_{L\text{-}1min\text{-}HL}$ is the CCF during a series of 1 min-HL-lightflecks [nine repeated cycles of 1 min of I_{inc} (incident irradiance) of 1500 µmol m^{-2} s^{-1} followed by 1 min of I_{inc} of 50 µmol m^{-2} s^{-1}]. $CCF_{L\text{-}1min\text{-}HL}$ is the CCF during a series of 1 min-LH-lightflecks (nine repeated cycles of 1 min of I_{inc} of 50 µmol m^{-2} s^{-1} followed by 1 min of I_{inc} of 1500 µmol m^{-2} s^{-1}). A_{ni} is the initial steady-state net photosynthetic rate (A_n) at I_{inc} of 50 µmol m^{-2} s^{-1} during a single-step irradiance increase; and A_{nf} is the final steady-state A_n at I_{inc} of 1500 µmol m^{-2} s^{-1} during a single-step irradiance increase. Statistical parameters given in the panels are in bold if data are combined for all treatments. The lines represent significant regressions (P<0.05).

2020), and (ii) the rate of photosynthetic induction was mainly limited by their biochemistry (Soleh *et al.*, 2016, 2017; Salter *et al.*, 2019; Acevedo-Siaca *et al.*, 2020, 2021). Our study contained the data allowing investigation of dynamic photosynthesis for rice during the whole growth cycle under ambient conditions over 2 years.

Our results showed that at all developmental stages, photosynthesis in leaves that were adapted to I_{inc} of 50 µmol m^{-2} s^{-1} for 30 min took ~600 s to reach a steady-state value after a single-step increase in irradiance to 1500 µmol m^{-2} s^{-1} (Supplementary Figs S4–S6). However, photosynthesis in leaves that were adapted to an I_{inc} of 1500 µmol m^{-2} s^{-1} for 30 min dropped below A_{ni} within 30 s after irradiance was switched back to 50 µmol m^{-2} s^{-1} (Supplementary Fig. S15). These results supported previous findings on the asymmetry of dynamic photosynthesis in response to light increases and drops—photosynthesis in leaves that were initially adapted to low irradiance increased relatively slowly in response to sudden increases in irradiance, but dropped almost immediately after decreases in irradiance (Chazdon and Pearcy, 1986a; Kaiser *et al.*, 2017b; Yamori *et al.*, 2020; Kang *et al.*, 2021). These asymmetries were also exhibited when plants were exposed to a series of lightflecks (Supplementary Figs S13, S15, S18). Our results showed that the overall LfUE during a series of lightflecks at all developmental stages was ~83% (Supplementary Tables S7, S8). This was largely due to the slow response of photosynthesis to sudden increases in irradiance (Supplementary Figs S13, S15, S18). In our case study, the LfUE of ~83% suggested that the slow response of photosynthesis to increases in irradiance cost ~17% of potential assimilation. Our results confirm that a fast rate of photosynthetic induction to fluctuating irradiance is a valuable trait for improving crop productivity.

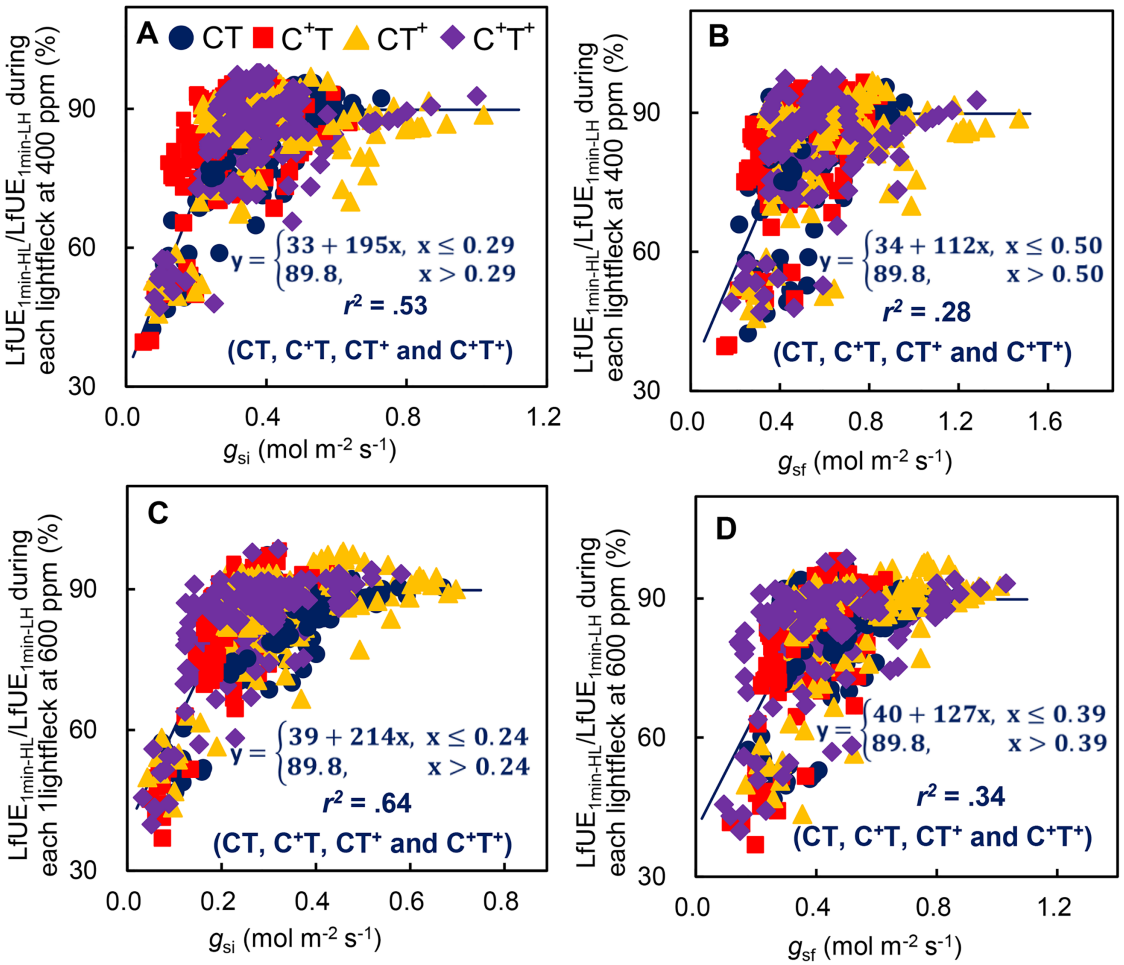

Fig. 5. Relationships between LfUE and g_{si} or g_{sf} in the 2023 experiment. Relationships between LfUE and g_{si} or g_{sf} during each lightfleck for ambient conditions (circles, CT), elevated CO_2 (squares, C^+T), elevated temperature (triangles, CT^+), and the combination of elevated CO_2 and elevated temperature (diamonds, C^+T^+) at all stages in the 2023 experiment. LfUE is lightfleck utilization efficiency. $LfUE_{1min\text{-}HL}$ is LfUE of 1 min-HL-lightfleck [1 min of I_{inc} (incident irradiance) of 1500 μmol m^{-2} s^{-1} followed by 1 min of I_{inc} of 50 μmol m^{-2} s^{-1}]. $LfUE_{1min\text{-}LH}$ is LfUE of 1 min-LH-lightfleck (1 min of I_{inc} of 50 μmol m^{-2} s^{-1} followed by 1 min of I_{inc} of 1500 μmol m^{-2} s^{-1}). g_{si} and g_{sf} are stomatal conductance at the onset and at the end of high irradiance in each lightfleck, respectively. As the relationships between LfUE and g_{si} or g_{sf} for each treatment did not differ significantly between each 1 min-HL-lightfleck and each 1 min-LH-lightfleck, each panel contains data for both lightfleck types. Statistical parameters given in the panels are in bold if data are combined for all treatments. These non-linear relationships between LfUE and g_{si} or g_{sf} differed significantly between the two measurement CO_2 levels (400 μmol mol^{-1} and 600 μmol mol^{-1}), but not between the two measurement leaf temperature levels (31 °C and 33 °C).

Parameter $IT_{50,A}$ or $IT_{90,A}$, whose inverse reflects the rate of photosynthetic induction, was significantly correlated with g_{si} during a single-step irradiance increase and lightflecks (Fig. 6; Supplementary Fig. S22). This was consistent with previous findings that values of $IT_{50,A}$ or $IT_{90,A}$ significantly correlated with g_{si} during a single-step irradiance increase (Allen and Pearcy, 2000a, b; Naumburg and Ellsworth, 2000; Kaiser *et al.*, 2016; Zhang *et al.*, 2022). In addition, we observed that $LfUE_{1min\text{-}HL}$, $LfUE_{3min\text{-}HL}$, and $LfUE_{1min\text{-}LH}$ were also significantly correlated with g_{si} (Fig. 5; Supplementary Fig. S23). Compared with photosynthesis, stomatal conductance dropped slowly after a single-step irradiance decrease (Supplementary Figs S4–S6). Stomatal conductance varied greatly during lightflecks (Supplementary Figs S14, S16, S19). A gradual increase in g_{si} (Supplementary Figs S14, S19) resulted in a gradual increase in LfUE (Fig. 3; Supplementary Figs S17, S20) depending on the number within the lightfleck series for both 1 min-HL-lightflecks and 3 min-HL-lightflecks at all developmental stages. Also, a slight decrease in g_{si} (Supplementary Fig. S16) resulted in a slight decrease in LfUE depending on the number within the lightfleck series for 1 min-LH-lightflecks at all developmental stages (Fig. 3; Supplementary Fig. S17). Higher g_{si} resulted in higher LfUE during a series of 1 min-HL-lightflecks than during a series of 3 min-HL-lightflecks (Supplementary Table S8; Supplementary Figs S19, S23). Furthermore, high g_{si} also resulted in higher LfUE during a series of 1 min-LH-lightflecks than during a series of 1 min-HL-lightflecks (Fig. 5; Supplementary Figs S14, S16; Supplementary Table S7). Our

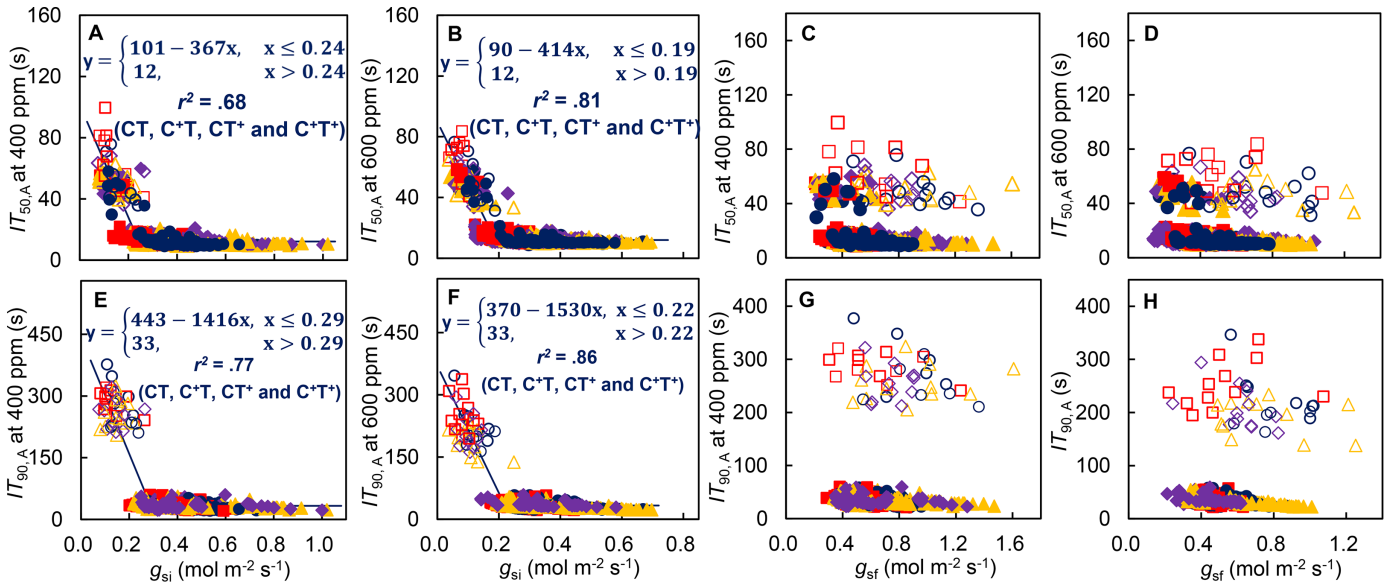

Fig. 6. Relationships between $IT_{50,A}$ and g_{si} or g_{sf}, and between $IT_{90,A}$ and g_{si} or g_{sf} in the 2023 experiment. Relationships between $IT_{50,A}$ and g_{si} or g_{sf}, and between $IT_{90,A}$ and g_{si} or g_{sf} during a single-step irradiance increase (open symbols) and during each lightfleck (closed symbols) for ambient conditions (circles, CT), elevated CO_2 (squares, C⁺T), elevated temperature (triangles, CT⁺), and the combination of elevated CO_2 and elevated temperature (diamonds, C⁺T⁺) at all stages in the 2023 experiment. $IT_{50,A}$ and $IT_{90,A}$ are the times required to reach 50% and 90%, respectively, of the full photosynthetic induction after the increase in irradiance or after exposure to high irradiance in each single lightfleck. g_{si} is the initial steady-state stomatal conductance at I_{inc} (incident irradiance) of 50 μmol m^{-2} s^{-1} in the case of a single-step irradiance increase, or stomatal conductance at the onset of high irradiance in the case of each lightfleck. g_{sf} is final steady-state stomatal conductance at I_{inc} of 1500 μmol m^{-2} s^{-1} in the case of a single-step irradiance increase, or stomatal conductance at the end of high irradiance in the case of each lightfleck. As this relationship between $IT_{50,A}$ or $IT_{90,A}$ and g_{si} for each treatment did not differ significantly between each lightfleck and single-step irradiance increase, all panels contain data for both a single-step irradiance increase and each lightfleck. The line was fitted for all data and represented significant regression (P<0.05). These non-linear relationships between $IT_{50,A}$ or $IT_{90,A}$ and g_{si} differed significantly between the two measurement CO_2 levels (400 μmol mol^{-1} and 600 μmol mol s^{-1}), but not between the two measurement leaf temperature levels (31 °C and 33 °C).

results suggested that g_s played a pivotal role in determining LfUE of dynamic photosynthesis for rice across developmental stages under ambient conditions.

Effect of growth CO_2 or growth temperature in T-FACE environments on dynamic photosynthesis

Our results showed that elevated growth CO_2 down-regulated $CCF_{I\text{-}600s}$, $CCF_{L\text{-}1min\text{-}HL}$, $CCF_{L\text{-}1min\text{-}LH}$, and steady-state photosynthesis for rice after flowering, by 8–10% (Figs 2F, N, 7B, F) (more details are available in Supplementary Tables S1–S4, S7, and S9). Elevated growth temperature marginally increased (by ~3%) $CCF_{D\text{-}60s}$ and $CCF_{I\text{-}600s}$ in the 2023 experiment (Fig. 2D, H), and A_{nf}, $CCF_{D\text{-}60s}$, $CCF_{I\text{-}600s}$, $CCF_{L\text{-}1min\text{-}HL}$, and $CCF_{L\text{-}3min\text{-}HL}$ in the 2021 experiment after flowering (Supplementary Figs S8A, D, J, S24A, B) (more details are given in Supplementary Tables S1–S4 and S8). These results suggest that not only steady-state but also dynamic photosynthesis after rice flowering acclimated strongly to elevated growth CO_2 but marginally to elevated growth temperature. Zhang *et al.* (2024) found that elevated growth CO_2 caused down-regulation of steady-state photosynthesis, but not of dynamic photosynthesis, for horticultural species. These findings indicate that the acclimation response of dynamic photosynthesis to elevated growth CO_2 differed among species. However, elevated growth CO_2 and growth temperature hardly affected photosynthetic induction rates (Supplementary Figs S9, S10) and LfUE (Fig. 7; Supplementary Fig. S24) during the whole cycle in both experiments. Kang *et al.* (2021) also reported that elevated growth CO_2 hardly affected rates of photosynthetic induction for rice and wheat.

Ohkubo *et al.* (2020) found that daily carbon gain during fluctuating irradiance was strongly correlated with steady-state photosynthesis. Our results showed that CCF during a single-step irradiance increase and during lightflecks was linearly correlated with A_{nf} in all treatments across all developmental stages in both experiments (Figs 1, 4; Supplementary Figs S8, S21). Furthermore, these linear relationships were not affected by elevated growth CO_2, or by growth temperature (Figs 1, 4; Supplementary Figs S8, S21). These results were in contrast to our first hypothesis that dynamic photosynthetic parameters strongly acclimated to elevated growth CO_2 and growth temperature. The effects of elevated growth CO_2 or growth temperature on CCF either during a single-step irradiance change or during lightflecks were quantitatively almost the same as their effects

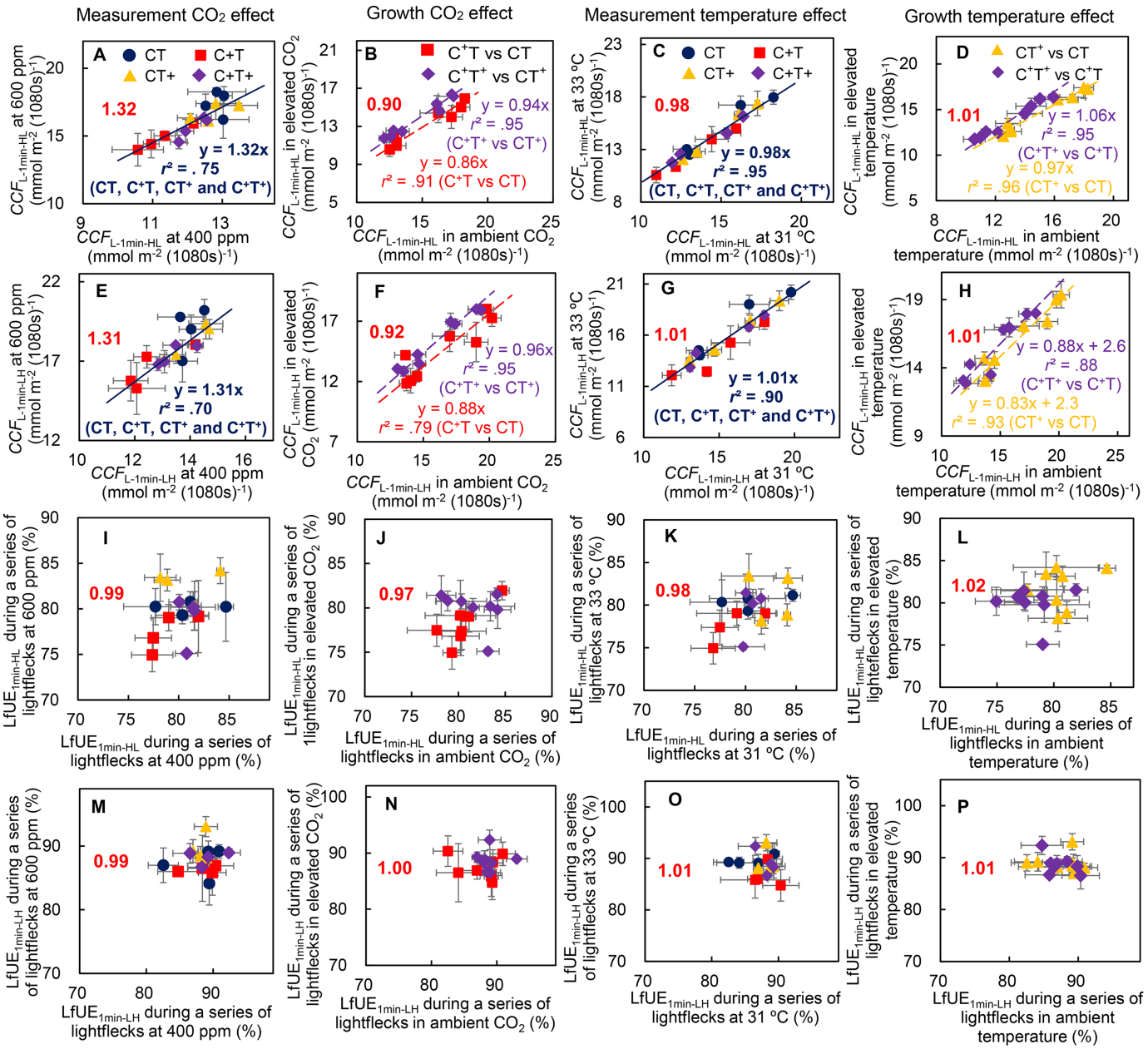

Fig. 7. Effects of measurement CO_2, growth CO_2, measurement temperature, and growth temperature on $CCF_{L\text{-}1min\text{-}HL}$, $CCF_{L\text{-}1min\text{-}LH}$, $LfUE_{1min\text{-}HL}$, and $LfUE_{1min\text{-}LH}$ in the 2023 experiment. Effects of measurement CO_2 (first column), growth CO_2 (second column), measurement temperature (third column), and growth temperature (fourth column) on $CCF_{L\text{-}1min\text{-}HL}$ (A–D), $CCF_{L\text{-}1min\text{-}LH}$ (E–H), $LfUE_{1min\text{-}HL}$ (I–L), and $LfUE_{1min\text{-}LH}$ (M–P) during a series of lightflecks in the 2023 experiment. $CCF_{L\text{-}1min\text{-}HL}$ is the cumulative CO_2 fixation (CCF) during a series of 1 min-HL-lightflecks [nine repeated cycles of 1 min of I_{inc} (incident irradiance) of 1500 μmol m^{-2} s^{-1} followed by 1 min of I_{inc} of 50 μmol m^{-2} s^{-1}]. $CCF_{L\text{-}1min\text{-}LH}$ is the *CCF* during a series of 1 min-LH-lightflecks (nine repeated cycles of 1 min of I_{inc} of 50 μmol m^{-2} s^{-1} followed by 1 min of I_{inc} of 1500 μmol m^{-2} s^{-1}). $LfUE_{1min\text{-}HL}$ is the lightfleck utilization efficiency (LfUE) during a series of 1 min-HL-lightflecks. $LfUE_{1min\text{-}LH}$ is the LfUE during a series of 1 min-LH-lightflecks. Each data point is the mean value ±SE of three replications. Statistical parameters given in the panels are in bold if the lines were fitted for all data. The lines represent significant linear regressions (P<0.05). The bold number in red in each panel is the average ratio of *y*-axis to *x*-axis values.

on A_{nf} during the whole cycle in both experiments (Figs 2, 7; Supplementary Figs S10, S24). This was due to the small effect of elevated growth CO_2 or growth temperature on photosynthetic induction rates and LfUE. Thus, the acclimation of dynamic photosynthesis to elevated growth CO_2 or growth temperature was related to that of steady-state photosynthesis at high irradiance.

The rate of photosynthetic induction is believed to be mainly regulated by four categories of processes, namely induction of electron transport rates, of Calvin cycle enzyme

activities, of stomatal opening, and of mesophyll conductance (Pearcy, 1990; Tomimatsu and Tang, 2016; Yamori, 2016; Zeng *et al.*, 2024). We further investigated which physiological factor played a role in determining the rate of photosynthetic induction and LfUE in response to elevated growth CO_2 and growth temperature. Our results showed that photosynthetic induction rates were weakly correlated with the induction rates of biochemical parameters across developmental stages in both experiments (Supplementary Figs S11, S12). However, both $IT_{50,A}$ and $IT_{90,A}$ were very significantly correlated with g_{si} during a single-step irradiance increase and during lightflecks for all treatments in both experiments (Fig. 6; Supplementary Fig. S22). Furthermore, these relationships for $IT_{50,A}$ and $IT_{90,A}$ were not affected by elevated growth CO_2, or by growth temperature in the 2023 experiment (Fig. 6). In addition, the significant relationship between LfUE and g_{si} was also not affected by elevated growth CO_2, or by growth temperature in the 2023 experiment (Fig. 5). These results are in contrast to our other hypothesis that both biochemical parameters and stomatal conductance controlled the response rate of photosynthesis during induction and during lightflecks in response to elevated growth CO_2 and growth temperature. Our results suggested instead that only stomatal conductance played a pivotal role.

Effect of combined elevated growth CO_2 and temperature on dynamic photosynthesis

Future climate change is associated with both elevated CO_2 and elevated temperature. Our T-FACE systems provided a unique opportunity to explore the effects of combined growth CO_2 and temperature on dynamic photosynthesis and its relationship to steady-state photosynthesis under future climate conditions. Our results in both experiments showed that combined growth CO_2 and temperature (C^+T^+) notably decreased CCF during a single-step irradiance increase and during lightflecks after flowering, compared with the ambient conditions (CT) (Supplementary Tables S1, S3, S7). This decrease was largely caused by elevated growth CO_2, and less by elevated growth temperature (Supplementary Tables S1, S3, S7). There was some interaction between growth CO_2 and growth temperature for CCF during a single-step irradiance increase at the grain-filling stage in the 2023 experiment (Supplementary Table S2), in line with our previous study (Cai *et al.*, 2018) that also observed a significant interaction between growth CO_2 and growth temperature for rice steady-state photosynthesis at high irradiance in T-FACE experiments. However, the interaction was not observed in the 2021 experiment (Supplementary Table S4). C^+T^+ did not alter the linear relationship between CCF and A_{nf} during a single-step irradiance change and during lighflecks in both experiments, compared with CT (Figs 1, 4; Supplementary Figs S8, S21).

There were significant interactions between growth CO_2 and growth temperature for $IT_{50,A}$ at the flowering stage in the 2023 experiment (Supplementary Table S2) and for $IT_{90,A}$ at the stem-elongation stage in the 2021 experiment (Supplementary Table S4). In addition, we also observed significant interactions between growth CO_2 and growth temperature for $IT_{50,J}$ and $IT_{90,J}$ at the stem-elongation stage in the 2021 experiment (Supplementary Table S6). Previous studies suggested that the rate of photosynthetic induction was mainly limited by their biochemistry under ambient conditions (Soleh *et al.*, 2016, 2017; Salter *et al.*, 2019; Acevedo-Siaca *et al.*, 2020, 2021). This was inconsistent with our results (Supplementary Figs S11, S12). Our results showed that compared with CT, C^+T^+ did not alter the significant relationship between $IT_{50,A}$, $IT_{90,A}$, or LfUE and g_{si} across all measurement CO_2 levels, measurement temperature levels, and developmental stages in the 2023 experiments (Figs 5, 6). For lightflecks, values of g_{si} under C^+T^+ after the second exposure to 1 min-HL-lightflecks and 1 min-LH-lightflecks at all developmental stages were above or close to the threshold g_{si} for $LfUE_{1min\text{-}HL}$ and $LfUE_{1min\text{-}LH}$ in the 2023 experiment (Fig. 6; Supplementary Figs S14, S16). During a single-step irradiance increase in both experiments, C^+T^+ hardly affected IT_{50A} and IT_{90A} across all measurement CO_2 levels, measurement temperature levels, and developmental stages, compared with CT (Supplementary Tables S1, S3). Taken together, the combined growth CO_2 and temperature slightly affected rates of photosynthetic induction and LfUE in both experiments. Thus, the effects of the combined growth CO_2 and temperature on CCF either during a single-step irradiance or during lightflecks were almost the same as their combined effect on steady-state photosynthesis at high irradiance.

Effect of measurement CO_2 or measurement temperature on dynamic photosynthesis

Elevated measurement CO_2 increases both steady-state and dynamic photosynthesis (Tomimatsu *et al.*, 2014; Kaiser *et al.*, 2017b; Kang *et al.*, 2021), consistent with our results of a 31–34% increase in both experiments (Figs 2, 7; Supplementary Fig. S10). However, the effects of elevated measurement temperature on these photosynthetic parameters during the whole cycle were very small in the 2023 experiment (Figs 2, 7). Linear regression analysis showed that neither elevated measurement CO_2 nor measurement temperature altered the linear relationships between CCF and A_{nf} during single-step irradiance change (Fig. 1; Supplementary Fig. S8) and during lightflecks (Fig. 4; Supplementary Fig. S21) in both years, in contrast to one of our hypotheses that responses of integrated dynamic photosynthesis to elevated measurement CO_2 and temperature were not correlated with those of steady-state photosynthesis. Further analysis indicated that the effect of elevated measurement CO_2 or measurement temperature on dynamic photosynthesis during a single-step irradiance increase and during lightflecks could be accurately predicted by their effect on steady-state photosynthesis at high irradiance in both experiments (Figs 2, 7; Supplementary Fig. S10).

Previous studies showed that elevated measurement CO_2 increased dynamic photosynthesis beyond its effects on steady-state photosynthesis, most of which was due to an increase in rate of photosynthetic induction (Tomimatsu *et al.*, 2014; Kaiser *et al.*, 2017b). However, reported responses of the photosynthetic induction rate to elevated measurement CO_2 were inconsistent (Tomimatsu *et al.*, 2014; Kaiser *et al.*, 2017b; Kang *et al.*, 2021). These resulted in inconsistent effects of elevated measurement CO_2 on dynamic versus steady-state photosynthesis (Tomimatsu *et al.*, 2014; Kaiser *et al.*, 2017b; Kang *et al.*, 2021). Kaiser *et al.* (2017b) found that measurement CO_2 elevation by 400 μmol mol^{-1} significantly decreased $IT_{50,A}$ and $IT_{90,A}$ by 37–61%, which additionally contributed 12% of the increased carbon gain for tomato. Tomimatsu *et al.* (2014) found that measurement CO_2 elevation by 350 μmol mol^{-1} significantly decreased $IT_{50,A}$, but not $IT_{90,A}$, which additionally contributed 7% of the increased carbon gain for *Dipterocarpus sublamellatus* seedlings. Our results for rice showed that the enhancement effect of measurement CO_2 elevation by 200 μmol mol^{-1} on $CCF_{L\text{-}600s}$ was only 3–4% higher, and that on $CCF_{L\text{-}1min\text{-}HL}$ and $CCF_{L\text{-}1min\text{-}LH}$ were 1% lower, than that on A_{nf} (Figs 2, 7; Supplementary Fig. S10). These were related to a slight decrease in $IT_{50,A}$ and $IT_{90,A}$ by 7–20% and in $LfUE_{1min\text{-}HL}$ and $LfUE_{1min\text{-}LH}$ during a series of lightflecks by 1% during the whole cycle (Fig. 7; Supplementary Figs S9, S10). The reason for these different results could be linked to the magnitude of the increase in measurement CO_2, differences in species used, and open field versus closed compartment conditions. We also showed that measurement temperature elevation by 2 °C had very small effects on rates of photosynthetic induction during a single-step irradiance increase and LfUE during lightflecks for all treatments in the 2023 experiment (Fig. 7; Supplementary Fig. S9). Thus, the effects of measurement temperature elevation on CCF during a single-step irradiance change and during lightflecks were of almost the same extent as its effect on steady-state photosynthesis at high irradiance (Figs 2, 7).

Rates of photosynthetic induction and LfUE in each lightfleck were strongly correlated with g_{si} in all treatments in both experiments (Figs 5, 6; Supplementary Figs S22, S23). Stomatal conductance during fluctuating irradiance was often reported to be notably decreased by elevated measurement CO_2 for C_3 crops (Kang *et al.*, 2021; Zhang *et al.*, 2024), consistent with our results in the 2023 experiment (Supplementary Figs S14, S16). However, elevated measurement CO_2 slightly affected $LfUE_{1min\text{-}HL}$ and $LfUE_{1min\text{-}LH}$ during a series of lightflecks in all treatments in the 2023 experiment (Fig. 7). The reason for this is probably 2-fold. Firstly, elevated measurement CO_2 significantly altered the non-linear relationship between $IT_{50,A}$, $IT_{90,A}$, $LfUE_{1\text{-}min\text{-}HL}$, or $LfUE_{1min\text{-}LH}$ and g_{si} in each lightfleck in the 2023 experiment (Figs 5, 6). For a given g_{si} below the threshold g_{si}, elevated measurement CO_2 decreased $IT_{50,A}$ or $IT_{90,A}$, but increased $LfUE_{1min\text{-}HL}$ and $LfUE_{1min\text{-}LH}$ in the 2023 experiment (Figs 5, 6). These might be related to a decrease in stomatal limitation caused by elevated measurement CO_2 (Kaiser *et al.*, 2015). Secondly, values of g_{si} at an elevated measurement CO_2 level (600 mmol mol^{-1}) for all treatments after the second exposure to 1 min-HL-lightflecks and 1 min-LH-lightflecks at all stages were above or close to the threshold g_{si} for $LfUE_{1min\text{-}HL}$ and $LfUE_{1min\text{-}LH}$ in the 2023 experiment (Fig. 5; Supplementary Figs S14, S16). In addition, elevated measurement temperature did not alter the non-linear relationship between $IT_{50,A}$, $IT_{90,A}$, $LfUE_{1min\text{-}HL}$, or $LfUE_{1min\text{-}LH}$ and g_{si} in each lightfleck (Figs 5, 6). Across all treatments during the whole cycle in 2023, elevated measurement temperature had slight effects on g_{si} (Supplementary Figs S14, S16), and thus on LfUE during 1 min-HL-lightflecks (Fig. 7K) and 1 min-LH-lightflecks (Fig. 7O).

Implications for modelling dynamic photosynthesis under future climate change

Many modelling results showed that the current crop model integrated with a steady-state photosynthesis model could predict crop growth and yield under both ambient field conditions and future field conditions very well (Yin, 2013; Hasegawa *et al.*, 2017; Li *et al.*, 2022). These could be supported by our results showing that CCF during a single-step change in irradiance or during lightflecks was positively correlated with A_{nf} or A_{ni} for the four CO_2 and temperature treatments during the whole crop cycle (Figs 1, 4). Zhang *et al.* (2022) found that the average photosynthesis during the first 300 s of induction had significant positive correlations with A_{nf} or A_{ni} for major horticultural crops under ambient conditions. Ohkubo *et al.* (2020) found that steady-state photosynthesis was strongly correlated with daily carbon gain during fluctuating irradiance for rice under ambient conditions.

However, LfUE, the ratio of CCF to assimilation expected from equivalent steady-state irradiance levels, changed from 44.5% to 94.7% depending on the number within the lightfleck series for all treatments (Fig. 3; Supplementary Figs S17, S20). This was a consequence of changes in rates of photosynthetic induction with the number within the lightfleck series for all treatments. Previous studies showed that the rate of photosynthetic induction strongly depends on the recent light history of the leaf (Kaiser *et al.*, 2016, 2017a) and is affected by environmental factors (such as temperature, air humidity, leaf-to-air vapour pressure difference, and CO_2 concentration) (Kaiser *et al.*, 2015, 2017a). Our results showed that both LfUE in each lightfleck and rates of photosynthetic induction were more significantly correlated with g_{si} than with g_{sf} for four CO_2 and temperature treatments in rice across all developmental stages (Figs 5, 6; Supplementary Figs S22, S23). Elevated CO_2 and temperature strongly affected g_s at both high and low irradiance during lightflecks (Supplementary Figs S14, S16, S19). Zhang *et al.* (2022) also found that $IT_{50,A}$ and $IT_{90,A}$ were significantly correlated with g_{si}, but not with g_{sf} for major horticultural crops under

ambient conditions. Thus, g_{si} played a pivotal role in determining carbon gain during fluctuating irradiance (Allen and Pearcy, 2000a, b; Urban *et al.*, 2007, 2008; Kaiser *et al.*, 2016). In contrast, photosynthetic induction rates were only weakly correlated with the induction rates of biochemical parameters (Supplementary Figs S11, S12). Thus, neglecting the effects of elevated CO_2 and temperature on induction rates of biochemical parameters did not result in critical errors in predicting dynamic photosynthesis under future climate change. Previous studies showed that mesophyll conductance played an important role in limiting photosynthesis during induction under ambient conditions (Liu *et al.*, 2022) and combined drought and heat stresses (Zeng *et al.*, 2024). Our previous studies showed that elevated CO_2 and temperature decreased steady-state mesophyll conductance (Cai *et al.*, 2018, 2020). However, the effects of elevated CO_2 and temperature on induction kinetics of mesophyll conductance remain to be quantified. Overall, a biochemical model for steady-state photosynthesis can be used to accurately predict dynamic photosynthesis in responses to elevated CO_2 and temperature under a future natural environment, provided that stomatal conductance, especially g_{si}, in responses to fluctuating irradiance can be quantified reliably.

Conclusion

This study examined the responses of rice dynamic photosynthesis to elevated CO_2 and temperature during the whole growth cycle in T-FACE experiments in 2 years. Our results showed that the CCF during a single-step irradiance increase and during lightflecks acclimated strongly to elevated growth CO_2 but marginally to growth temperature. The acclimations of CCF during a single-step irradiance increase and during lightflecks to elevated growth CO_2 and growth temperature were correlated with those of final steady-state photosynthesis at high irradiance (A_{nf}). The effects of elevated growth CO_2, elevated measurement CO_2, elevated growth temperature, and elevated measurement temperature on CCF during a single-step irradiance increase and during lightflecks were of almost the same extent as their effects on A_{nf}. Photosynthetic induction rates during a single-step irradiance increase and during each lightfleck in the four CO_2 and temperature treatments were strongly correlated with initial stomatal conductance, but were only weakly correlated with the induction rates of biochemical parameters. LfUE showed a large variation dependent on the number within the lightfleck series. This was related to the variation of stomatal conductance among the series of numbers. Our results suggest that steady-state photosynthesis models can be used to accurately predict dynamic photosynthesis in response to elevated CO_2 and temperature under future climatic conditions, provided that stomatal conductance in response to fluctuating irradiance can be quantified reliably.

Supplementary data

The following supplementary data are available at *JXB* online.

Fig. S1. The T-FACE system used in the 2023 experiment.

Fig. S2. Daily weather during the growing season for rice in 2021 and 2023.

Fig. S3. Measured and predicted time course of CO_2 assimilation during single lightflecks.

Fig. S4. Examples of changes in rice photosynthetic induction and stomatal conductance after a single-step change in irradiance at a leaf temperature of 31 °C in the 2023 experiment.

Fig. S5. Examples of changes in rice photosynthetic induction and stomatal conductance after a single-step change in irradiance at leaf temperature of 33 °C in the 2023 experiment.

Fig. S6. Changes in rice photosynthetic induction and stomatal conductance after a single-step change in irradiance in the 2021 experiment.

Fig. S7. Relationships between $IT_{50,A}$ and A_{ni} or A_{nf}, between $IT_{90,A}$ and A_{ni} or A_{nf}, and between A_{nf} and A_{ni} during a single-step change in irradiance in the 2023 experiment.

Fig. S8. Relationships among photosynthetic parameters during a single-step change in irradiance in the 2021 experiment.

Fig. S9. Effects of measurement CO_2, growth CO_2, measurement temperature, and growth temperature on g_{si}, g_{sf}, $IT_{50,A}$, and $IT_{90,A}$ during a single-step irradiance increase in the 2023 experiment.

Fig. S10. Effects of measurement CO_2, growth CO_2, and growth temperature on photosynthetic parameters during a single-step irradiance increase in the 2021 experiment.

Fig. S11. Relationships between $IT_{50,A}$ and $IT_{50,Vcmax}$ or $IT_{50,J}$, and between $IT_{90,A}$ and $IT_{90,Vcmax}$ or $IT_{90,J}$ in the 2023 experiment.

Fig. S12. Relationships between $IT_{50,A}$ and $IT_{50,Vcmax}$ or $IT_{50,J}$, and between $IT_{90,A}$ and $IT_{90,Vcmax}$ or $IT_{90,J}$ in the 2021 experiment.

Fig. S13. Time courses of rice photosynthetic response to a series of 1 min-HL-lightflecks in the 2023 experiment.

Fig. S14. Time courses of rice stomatal conductance response to a series of 1 min-HL-lightflecks in the 2023 experiment.

Fig. S15. Time courses of rice photosynthetic response to a series of 1 min-LH-lightflecks in the 2023 experiment.

Fig. S16. Time courses of rice stomatal conductance response to a series of 1 min-LH-lightflecks in the 2023 experiment.

Fig. S17. Rice lightfleck utilization efficiency during the first to ninth 1 min-HL-lightflecks and during 1 min-LH-lightflecks at a leaf temperature of 33 °C in the 2023 experiment.

Fig. S18. Time courses of rice photosynthetic response to a series of 1 min-HL-lightflecks and 3 min-HL-lightflecks in the 2021 experiment.

Fig. S19. Time courses of rice stomatal conductance response to a series of 1 min-HL-lightflecks and 3 min-HL-lightflecks in the 2021 experiment.

Fig. S20. Rice lightfleck utilization efficiency during the first to ninth 1 min-HL-lightflecks and during the first to third 3 min-HL-lightflecks in the 2021 experiment.

Fig. S21. Relationships between CCF_L and A_{nf} or A_{ni} in the 2021 experiment.

Fig. S22. Relationships between $IT_{50,A}$ and g_{si} or g_{sf}, and between $IT_{90,A}$ and g_{si} or g_{sf} during a single-step increase in irradiance and during each lightfleck in the 2021 experiment.

Fig. S23. Relationships between LfUE and A_{nf} or A_{ni} in the 2021 experiment.

Fig. S24. Effects of growth temperature on rice CCF_L and LfUE in the 2021 experiment.

Table S1. Photosynthetic parameters during induction in the 2023 experiment.

Table S2. ANOVA of measurement CO_2, growth CO_2, measurement temperature, and growth temperature effects on photosynthetic parameters during induction in the 2023 experiment.

Table S3. Photosynthetic parameters during induction in the 2021 experiment.

Table S4. ANOVA of measurement CO_2, growth CO_2, and growth temperature effects on photosynthetic parameters during induction in the 2021 experiment.

Table S5. Time for 50% and 90% induction of V_{cmax} or of J in the 2023 experiment.

Table S6. Time for 50% and 90% induction of V_{cmax} or of J in the 2021 experiment.

Table S7. The cumulative CO_2 fixation and lightfleck utilization efficiency during a series of 1 min-HL-lightflecks and 1 min-LH-lightflecks in the 2023 experiment.

Table S8. The cumulative CO_2 fixation and lightfleck utilization efficiency during a series of 1 min-HL-lightflecks and 3 min-HL-lightflecks in the 2021 experiment.

Table S9. Analysis of measurement CO_2, growth CO_2, measurement temperature, and growth temperature effects on the cumulative CO_2 fixation and lightfleck utilization efficiency during a series of 1 min-HL-lightflecks and 1 min-LH-lightflecks in the 2023 experiment.

Protocol S1. The FvCB model.

Acknowledgements

Many thanks go to Dr Xiaoyu Liu of the College of Resources and Environmental Science, Nanjing Agricultural University, Faqing Wang of the Institute of Soil Science, Chinese Academy of Sciences, and Haizeng Li of Sheng Yan Electronic Technology Co., Ltd for their technical support during the T-FACE experiments.

Author Contributions

CC and CWZ: conceived and designed the experiment; CC, XYG, and XY: performed the experiment; CC and XYY: analysed data and wrote the manuscript; XYY, CC, CWZ, XGZ, LS, and WZ: revised the manuscript.

Conflict of interest statement

The authors declare no conflicts of interest.

Funding

This research was funded by the China Natural Science Foundation (32171591, 32001191, and 42071050), the China Postdoctoral Science Foundation (2020M681751 and 2020T130663), the Carbon Peaking and Carbon Neutrality Special Fund for Science and Technology from Nanjing Science and Technology Bureau (20221103), the Science Foundation of the Chinese Academy of Sciences (ISSAS2413), the '0 to 1' original innovation project of the Basic Frontier Science Research Program of CAS (ZDBS-LY-DQC020), the National Key Research and Development Program of China (no. 2023YFD1500801), the Major Science and Technology Project of Ordos City (2022EEDSKJZDZX010), and the Key-Area Research and Development Program of Guangdong Province, China (no. 2020B0202010006).

Data availability

All data supporting the findings of this study are available within the paper and within its supplementary data. Further inquiries can be directed to the corresponding author (Chunwu Zhu).

References

Acevedo-Siaca LG, Coe R, Quick WP, Long SP. 2021. Variation between rice accessions in photosynthetic induction in flag leaves and underlying mechanisms. Journal of Experimental Botany **72**, 1282–1294.

Acevedo-Siaca LG, Coe R, Wang Y, Kromdijk J, Quick WP, Long SP. 2020. Variation in photosynthetic induction between rice accessions and its potential for improving productivity. New Phytologist **227**, 1097–1108.

Adachi M, Hasegawa T, Fukayama H, Tokida T, Sakai H, Matsunami T, Nakamura H, Sameshima R, Okada M. 2014. Soil and water warming accelerates phenology and down-regulation of leaf photosynthesis of rice plants grown under free-air CO_2 enrichment. Plant and Cell Physiology **55**, 370–380.

Allen MT, Pearcy RW. 2000a. Stomatal behaviour and photosynthetic performance under dynamic light regimes in a seasonally dry tropical rain forest. Oecologia **122**, 470–478.

Allen MT, Pearcy RW. 2000b. Stomatal versus biochemical limitations to dynamic photosynthetic performance in four tropical rainforest shrub species. Oecologia **122**, 479–486.

Alonso A, Pérez P, Martínez-Carrasco R. 2009. Growth in elevated CO_2 enhances temperature response of photosynthesis in wheat. Physiologia Plantarum **135**, 109–120.

Borjigidai A, Hikosaka K, Hirose T, Hasegawa T, Okada M, Kobayashi K. 2006. Seasonal changes in temperature dependence of photosynthetic rate in rice under a free-air CO_2 enrichment. Annals of Botany **97**, 549–557.

Cai C, Li G, Di L, *et al*. 2020. The acclimation of leaf photosynthesis of wheat and rice to seasonal temperature changes in T-FACE environments? Global Change Biology **26**, 539–556.

Cai C, Li G, Yang H, *et al*. 2018. Do all leaf photosynthesis parameters of rice acclimate to elevated CO_2, elevated temperature, and their combination, in FACE environments? Global Change Biology **24**, 1685–1707.

Cai C, Yin X, He S, *et al*. 2016. Responses of wheat and rice to factorial combinations of ambient and elevated CO_2 and temperature in FACE experiments. Global Change Biology **22**, 856–874.

Chazdon RL, Pearcy RW. 1986a. Photosynthetic responses to light variation in rainforest species: I. Induction under constant and fluctuating light conditions. Oecologia **69**, 517–523.

Chazdon RL, Pearcy RW. 1986b. Photosynthetic responses to light variation in rainforest species: II. Carbon gain and photosynthetic efficiency during lightflecks. Oecologia **69**, 524–531.

Ciais P, Sabine C, Bala G, *et al*. 2013. Carbon and other biogeochemical cycles. In: Tignor M, Allen SK, Boschung J, Nauels A, Xia Y, Bex V, Midgley PM, eds. Climate change 2013: the physical science basis. Contribution of Working Group I to the Fifth Assessment Report of the Intergovernamental Panel on Climate Change. Cambridge, UK and New York, USA: Cambridge University Press, 465–570.

Faralli M, Cockram J, Ober E, Wall S, Galle A, Van Rie J, Raines C, Lawson T. 2019. Genotypic, developmental and environmental effects on the rapidity of g_s in wheat: impacts on carbon gain and water-use efficiency. Frontiers in Plant Science **10**, 492.

Farquhar GD, von Caemmerer S, Berry JA. 1980. A biochemical model of photosynthetic CO_2 assimilation in leaves of C_3 species. Planta **149**, 78–90.

Hasegawa T, Li T, Yin X, *et al*. 2017. Causes of variation among rice models in yield response to CO_2 examined with free-air CO_2 enrichment and growth chamber experiments. Scientific Reports **7**, 14858.

Kaiser E, Kromdijk J, Harbinson J, Heuvelink E, Marcelis LFM. 2017a. Photosynthetic induction and its diffusional, carboxylation and electron transport processes as affected by CO_2 partial pressure, temperature, air humidity and blue irradiance. Annals of Botany **119**, 191–205.

Kaiser E, Morales A, Harbinson J, Heuvelink E, Kromdijk J, Marcelis LFM. 2016. Metabolic and diffusional limitations of photosynthesis in fluctuating irradiance in *Arabidopsis thaliana*. Scientific Reports **6**, 31252.

Kaiser E, Morales A, Harbinson J, Kromdijk J, Heuvelink E, Marcelis LFM. 2015. Dynamic photosynthesis in different environmental conditions. Journal of Experimental Botany **66**, 2415–2426.

Kaiser E, Zhou D, Heuvelink E, Harbinson J, Morales A, Marcelis LFM. 2017b. Elevated CO_2 increases photosynthesis in fluctuating irradiance regardless of photosynthetic induction state. Journal of Experimental Botany **68**, 5629–5640.

Kang H, Zhu T, Zhang Y, Ke X, Sun W, Hu Z, Zhu X, Shen H, Huang Y, Tang Y. 2021. Elevated CO_2 enhances dynamic photosynthesis in rice and wheat. Frontiers in Plant Science **12**, 727374.

Leakey ADB, Press MC, Scholes JD. 2003. High-temperature inhibition of photosynthesis is greater under sunflecks than uniform irradiance in a tropical rain forest tree seedling. Plant, Cell & Environment **26**, 1681–1690.

Leakey ADB, Press MC, Scholes JD, Watling JR. 2002. Relative enhancement of photosynthesis and growth at elevated CO_2 is greater under sunflecks than uniform irradiance in a tropical rain forest tree seedling. Plant, Cell & Environment **25**, 1701–1714.

Li Y, Hou R, Liu X, Chen Y, Tao F. 2022. Changes in wheat traits under future climate change and their contributions to yield changes in conventional vs. conservational tillage systems. The Science of the Total Environment **815**, 152947.

Liu T, Barbour MM, Yu D, Rao S, Song X. 2022. Mesophyll conductance exerts a significant limitation on photosynthesis during light induction. New Phytologist **233**, 360–372.

Long SP, Taylor SH, Burgess SJ, Carmo-Silva E, Lawson T, De Souza AP, Leonelli L, Wang Y. 2022. Into the shadows and back into sunlight: photosynthesis in fluctuating light. Annual Review of Plant Biology **73**, 617–648.

Naumburg E, Ellsworth DS. 2000. Photosynthesis sunfleck utilization potential of understory saplings growing under elevated CO_2 in FACE. Oecologia **122**, 163–174.

Ohkubo S, Tanaka Y, Yamori W, Adachi S. 2020. Rice cultivar Takanari has higher photosynthetic performance under fluctuating light than Koshihikari, especially under limited nitrogen supply and elevated CO_2. Frontiers in Plant Science **11**, 1308.

Pearcy RW. 1990. Sunflecks and photosynthesis in plant canopies. Annual Review of Plant Physiology and Plant Molecular Biology **41**, 421–453.

Pozo AD, Pérez P, Morcuende R, Alonso A, Martínez-Carrasco R. 2005. Acclimatory responses of stomatal conductance and photosynthesis to elevated CO_2 and temperature in wheat crops grown at varying levels of N supply in a Mediterranean environment. Plant Science **169**, 908–916.

Ruiz-Vera UM, Siebers MH, Drag DW, Ort DR, Bernacchi CJ. 2015. Canopy warming caused photosynthetic acclimation and reduced see yield in maize grown at ambient and elevated [CO_2]. Global Change Biology **21**, 4237–4249.

Salter W, Merchant AM, Richards RA, Trethowan R, Buckley TN. 2019. Rate of photosynthetic induction in fluctuating light varies widely among genotypes of wheat. Journal of Experimental Botany **10**, 2787–2796.

Smith WK, Berry ZC. 2013. Sunflecks? Tree Physiology **33**, 233–237.

Soleh MA, Tanaka Y, Kim SY, Huber SC, Sakoda K, Shiraiwa T. 2017. Identification of large variation in the photosynthetic induction response among 37 soybean [*Glycine max* (L.) Merr.] genotypes that is not correlated with steady-state photosynthetic capacity. Photosynthesis Research **131**, 305–315.

Soleh MA, Tanaka Y, Nomoto Y, Iwahashi Y, Nakashima K, Fukuda Y, Long SP, Shiraiwa T. 2016. Factors underlying genotypic differences in the induction of photosynthesis in soybean [*Glycine max* (L.) Merr.]. Plant, Cell & Environment **39**, 685–693.

Taniyoshi K, Tanaka Y, Shiraiwa T. 2020. Genetic variation in the photosynthetic induction response in rice (*Oryza sativa* L.). Plant Production Science **23**, 513–521.

Taylor SH, Long SP. 2017. Slow induction of photosynthesis on shade to sun transitions in wheat may cost at least 21% of productivity. Philosophical Transactions of the Royal Society B: Biological Sciences **372**, 20160543.

Tomimatsu H, Iio A, Adachi M, Saw L, Fletcher C, Tang Y. 2014. High CO_2 concentration increases relative leaf carbon gain under dynamic light in *Dipterocarpus sublamellatus* seedlings in a tropical rain forest, Malaysia. Tree Physiology **34**, 944–954.

Tomimatsu H, Tang Y. 2012. Elevated CO_2 differentially affects photosynthetic induction response in two *Populus* species with different stomatal behavior. Oecologia **169**, 869–878.

Tomimatsu H, Tang Y. 2016. Effects of high CO_2 levels on dynamic photosynthesis: carbon gain, mechanisms, and environmental interactions. Journal of Plant Research **129**, 365–377.

Urban O, Košvancová M, Marek MV, Lichtenthaler HK. 2007. Induction of photosynthesis and importance of limitations during the induction phase in sun and shade leaves of five ecologically contrasting tree species from the temperate zone. Tree Physiology **27**, 1207–1215.

Urban O, Šprtová M, Košvancová M, Tomášková I, Lichtenthaler HK, Marek MV. 2008. Comparison of photosynthetic induction and transient limitations during the induction phase in young and mature leaves from three poplar clones. Tree Physiology **28**, 1189–1197.

Usui Y, Sakai H, Tokida T, Nakamura H, Nakagawa H, Hasegawa T. 2016. Rice grain yield and quality responses to free-air CO_2 enrichment combined with soil and water warming. Global Change Biology **22**, 1256–1270.

Wang W, Yuan S, Wu C, *et al*. 2021. Field experiments and model simulation based evaluation of rice yield response to projected climate change in Southeastern China. The Science of the Total Environment **761**, 143206.

Yamori W. 2016. Photosynthetic response to fluctuating environments and photoprotective strategies under abiotic stress. Journal of Plant Research **129**, 379–395.

Yamori W, Kusumi K, Iba K, Terashima I. 2020. Increased stomatal conductance induces rapid changes to photosynthetic rate in response to naturally fluctuating light condition in rice. Plant, Cell & Environment **43**, 1230–1240.

Yin X. 2013. Improving ecophysiological simulation models to predict the impact of elevated atmospheric CO_2 concentration on crop productivity. Annals of Botany **112**, 465–475.

Yin X, Amthor JS. 2024. Estimating leaf day respiration from conventional gas exchange measurements. New Phytologist **241**, 52–58.

Yuan M, Cai C, Wang X, Li G, Wu G, Wang J, Geng W, Liu G, Zhu J, Sun Y. 2021. Warming air temperature increase photosynthetic acclimation

to elevated CO_2 concentrations in rice under field conditions. Field Crops Research **262**, 108036.

Zeng Z, Wang X, Zhang S, Huang W. 2024. Mesophyll conductance limits photosynthesis in fluctuating light under combined drought and heat stress. Plant Physiology **194**, 1498–1511.

Zhang N, Berman SR, Joubert D, Vialet-Chabrand S, Marcelis LFM, Kaiser E. 2022. Variation of photosynthetic induction in major horticultural crops is mostly driven by differences in stomatal traits. Frontiers in Plant Science **13**, 860229.

Zhang N, Berman SR, van den Berg T, Chen Y, Marcelis LFM, Kaiser E. 2024. Biochemical versus stomatal acclimation of dynamic photosynthetic gas exchange to elevated CO_2 in three horticultural species with contrasting stomatal morphology. Plant, Cell & Environment **47**, 4516–4529.